

Orthogonality catastrophe beyond Luttinger liquid from post-selection

Martino Stefanini and Jamir Marino

Institut für Physik, Johannes Gutenberg-Universität Mainz, D-55099 Mainz, Deutschland

(Dated: October 3, 2023)

We show that the dynamics induced by post-selected measurements can serve as a controlled route to access physical processes beyond the boundaries of Luttinger liquid physics. We consider a one-dimensional fermionic wire whose dynamics results from a sequence of weak measurements of the fermionic density at a given site, interspersed with unitary hopping dynamics. This realizes a non-Hermitian variant of the celebrated instance of a local scatterer in a fermionic system and its ensuing orthogonality catastrophe. We observe a distinct crossover in the system's time evolution as a function of the fermion density. In the high-density regime, reminiscent of the Hermitian case, Tomonaga-Luttinger liquid physics properly describes the dynamics while, as we delve into the low-density regime, the validity of bosonization breaks down, giving rise to irreversible behavior. Notably, this crossover from reversible to irreversible dynamics is non-perturbative in the measurement rate and can manifest itself even with relatively shallow measurement rates, provided that the system's density remains below the critical threshold. Our results render a conceptually transparent model for exploring non-perturbative effects beyond bosonization, which could be used as a step-stone to explore novel routes for the control of non-linear dynamics in low-dimensional quantum systems.

Introduction.— The Tomonaga-Luttinger liquid (TLL) stands as the universal, low-energy description for interacting one-dimensional (1D) quantum systems, renowned for its mathematical elegance and success in equilibrium scenarios [1, 2]. Its technical cornerstone, known as bosonization, allows to transform virtually any interacting system involving 1D fermions, bosons or spins into a massless free theory of collective bosonic excitations. Extending its applicability beyond equilibrium, especially in non-equilibrium settings, has been a topic of exploration in both isolated [3–10] and open systems [11–15], as well as in the realm of measurement-induced dynamics [16–18].

While the TLL framework proves remarkably robust even far from equilibrium in certain phenomenological cases [9, 13, 19–22], it lacks a formal renormalization group argument to guarantee its validity given the potential excitation of higher-energy degrees of freedom. The exploration of dynamics beyond TLL at equilibrium has seen significant attention in recent decades [23], yet understanding its validity in non-equilibrium conditions remains largely uncharted territory. This is partly due to the inherent technical challenges posed by the problem itself [24–26] and the absence of iconic models to guide such inquiries.

Nonetheless, delving into this line of inquiry holds both fundamental and practical significance. It serves as a potential testing ground for theories encompassing universal dynamics beyond traditional thermodynamics, while also offering the prospect of discovering effective models capable of simplifying the numerical resolution of highly correlated quantum dynamics.

In this Letter, we embark on an initial exploration in this direction by proposing a model of non-unitary dynamics where non-perturbative effects beyond Luttinger Liquid manifest in a controlled fashion, and where at

the same time the mechanisms for the breakdown of bosonization can be traced back to a transparent physical picture. Specifically, we implement a non-Hermitian version of the orthogonality catastrophe (OC) using post-selected continuous measurements of the local fermionic density at a given site. The OC [1, 2, 27, 28] is a paradigmatic phenomenon in solid-state physics, with countless applications ranging from the physics of X-rays [28, 29] to the Kondo effect [30], quantum dots [31, 32] and ultracold atoms [33–35]. The OC describes the strong sensitivity of gapless fermionic systems to local perturbations: a single scattering center introduced in a metal generates a new ground state which is orthogonal to the unperturbed one [27], due to the excitation of a diverging number of particle-hole pairs with vanishing energy. The dynamical signature of the OC is an algebraic decay of the return amplitude after turning on of the local potential. This characteristic decay has been proven by non-perturbative means [36, 37], but it is also predicted by a simple bosonized description [29]—an early example of a successful non-equilibrium application of bosonization.

In this study, we introduce a model where a local imaginary scattering potential is abruptly introduced into a noninteracting 1D fermionic system. While non-equilibrium versions of the OC problem have been explored in previous literature [38–41], our approach is distinct. We employ post-selection of measurements, which plays a pivotal role in our ability to control the extent to which the dynamics deviate from an effective bosonized description. Drawing inspiration from pioneering investigations of unitary versions of the OC, our primary focus is on the return amplitude, denoted as $\mathcal{L}(t) \equiv \langle \psi(0) | \psi(t) \rangle$. This quantity serves as a global indicator of how closely the full state aligns with the description provided by bosonization. Our findings re-

veal a distinct algebraic decay in $\mathcal{L}(t)$, consistent with the Hermitian scenario. However, in the non-Hermitian setting, we observe an additional exponential decay not anticipated by bosonization. Unlike conventional occurrences of decoherence in OC [38–40], this exponential decay signifies a reversible/irreversible dynamical crossover directly associated with the breakdown of bosonization. This feature stands as a unique hallmark of our post-selected implementation of the OC. The presence of a decay rate indicative of irreversible dynamics, strongly depends on the initial density of fermions: it is significant only in the low-density regime, where deviations from bosonization are notable, but tapers to zero as the background fermion density increases. This perspective is corroborated by our examination of the system’s kinetic energy, which exhibits linear growth over time. This growth hints at the existence of energy absorption processes that naturally drive deviations from the Luttinger liquid description whenever fermionic densities are low.

We interpret the breakdown of bosonization at low densities as a consequence of the presence of quasi-bound states in the single-particle spectrum of the non-Hermitian Hamiltonian that governs the dynamics. These states occur far from the Fermi surface, and exert their influence through the imaginary part of their eigenvalues. They exist because of the curvature of the fermionic dispersion, and so they disappear as the dispersion is linearized when bosonizing the Hamiltonian.

Model.— We consider a 1D system of noninteracting, spinless fermions c_j that can hop on the lattice sites of a chain according to the Hamiltonian $H = -J \sum_{j=0}^{L-1} (c_{j+1}^\dagger c_j + c_j^\dagger c_{j+1}) = \sum_q \varepsilon_q c_q^\dagger c_q$. The chain has L sites with periodic boundary conditions (pbc) and unit lattice spacing $a = 1$. We also use units such that $\hbar = 1$. The momentum modes are $c_q = L^{-1/2} \sum_j e^{-iqj} c_j$, corresponding to energies $\varepsilon_q \equiv -2J \cos q$.

We assume that the system is initialized in its ground state $|FS\rangle$ (at a certain filling N_f , namely density $\bar{n} = N_f/L$), and then evolves according to the nonlinear Schrödinger equation

$$i \frac{d}{dt} |\psi(t)\rangle = \left[K + i \frac{\gamma}{2} \langle \psi(t) | n_0 | \psi(t) \rangle \right] |\psi(t)\rangle, \quad (1)$$

where γ is a constant that can be of either sign, $n_0 \equiv c_{j_0}^\dagger c_{j_0}$ is the density at the site j_0 , and where we have introduced the non-Hermitian Hamiltonian

$$K \equiv H - i \frac{\gamma}{2} n_0. \quad (2)$$

The above Hamiltonian describes scattering off a localized potential (i.e. an impurity) that has an imaginary strength. It can be seen as the simplest non-Hermitian generalization of the OC problem. Equation (1) can be solved as $|\psi(t)\rangle = |\tilde{\psi}(t)\rangle / \langle \tilde{\psi}(t) | \tilde{\psi}(t) \rangle^{1/2}$, where $|\tilde{\psi}(t)\rangle = e^{-iKt} |\psi(0)\rangle$, so that the dynamics is simply the

normalized version of the non-unitary evolution generated by K .

There are several scenarios that lead to the dynamics (1), and all of them have in common some form of post-selection. We briefly present here a few of the simplest strategies, leaving a more detailed discussion to the Supplementary Material [42].

The most natural scenario is that of continuous monitoring [43, 44]: the system undergoes a series of weak measurements of the density at site j_0 at a rate γ , interspersed with Hamiltonian evolution, with a set of measurement operators that includes

$$M(\delta t) = \mathcal{N} e^{-\frac{\gamma \delta t}{2} n_0}, \quad (3)$$

along with other operators that we do not need to specify here (\mathcal{N} is a suitable normalization constant that plays no role). Such dynamics would yield stochastic state trajectories, conditioned on the random measurement outcomes, and Eq. (1) is obtained by selecting only those trajectories in which the outcome is always the one corresponding to the action of (3). This procedure is known as the “no-click” limit [16, 45–47]. Physically, the measurement operator (3) for $\gamma > 0$ may be taken to represent a measurement that has found no particles at j_0 , since it favors states with $n_0 = 0$. Vice versa, $\gamma < 0$ represents a measurement that finds one particle at j_0 .

It is also possible to simulate Eq. (1) with a dissipative dynamics governed by a Lindblad master equation, if the jump operator \mathcal{J} [43, 48] is such that the non-Hermitian part of the dissipative dynamics $\tilde{H} = H - i \frac{\gamma}{2} \mathcal{J}^\dagger \mathcal{J}$ reproduces Eq. (2) and a suitable post-selection of experimental runs is performed. The setup of a localized single particle loss $\mathcal{J} = c_{j_0}$ [14, 49–51] satisfies these criteria. Then, for each time t of the dynamics, the total number of particles is measured and only the runs in which no fermions have been lost are kept. The observables measured within this set of runs corresponds to the state $|\tilde{\psi}(t)\rangle$, and must be divided by its squared norm, which is simply the probability of not losing particles in the time t . This route can be followed in actual experiments (e.g. see [52] and [53]) for any dissipative dynamics for which there is a way to recognize the effect of dissipative events, the so-called jumps [48]. For instance, this procedure is possible for localized single particle gain $\mathcal{J} = c_{j_0}^\dagger$ [54], which corresponds to $\gamma < 0$, while it is not viable for localized dephasing $\mathcal{J} = n_0$ [38, 55].

A different dissipative strategy is to use an immobile impurity particle that induces a localized two-body loss [56–58] in the system, i.e. $\mathcal{J} = d c_{j_0}$, where d annihilates the impurity. Then, the effective Hamiltonian $\tilde{H} = H - i \gamma / 2 n_0 d^\dagger d$ can be switched from H to K by simply injecting the impurity, $d^\dagger d = 1$. Then, in analogy with the Hermitian scenario [34], one only needs to measure observables of the impurity to reconstruct the dynamics (1).

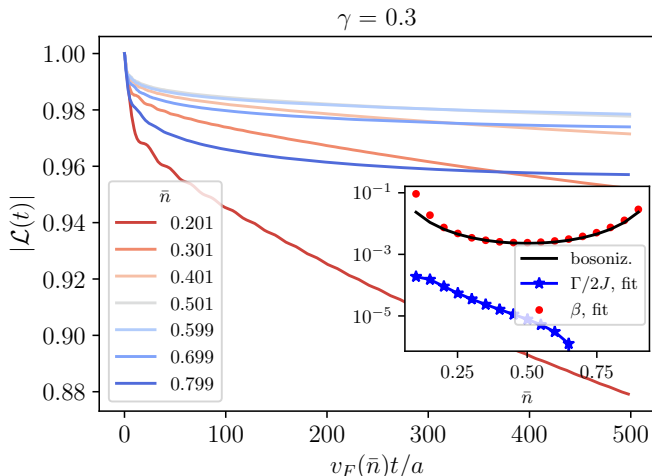


FIG. 1. Absolute value of the return amplitude as a function of the rescaled time for $L = 1000$, $J = 0.5$, $\gamma = 0.3$ and increasing density. The plot shows the absence of particle-hole symmetry as the low-density curves (in shades of red) decay faster than those at the conjugate densities $1 - \bar{n}$ (shades of blue) because of an additional exponential envelope caused by the post-selected measurements. Inset: filling dependence of the two fitting parameters β (OC exponent, red dots) and Γ (exponential decay rate, blue stars), along with the bosonization prediction for β (black line). The uncertainty on the fitted parameters is smaller than the size of the marker points.

Numerical evidences.— We have computed the time evolution of the system using the algorithm described in Ref. [59]: we evolve the matrix of the single-particle wavefunctions $U_{ji} = [\phi_{p_i}(j)]_{j=1, \dots, N_f}^{i=1, \dots, N_f}$ with the single-particle versions of H and M , and we keep the state normalized at each step.

We focus here on two main observables: the return amplitude and the total energy. The return amplitude is defined as $\mathcal{L}(t) \equiv \langle \psi(0) | \psi(t) \rangle = \langle FS | \psi(t) \rangle$, which is variously known as fidelity, Loschmidt echo or impurity Green's function. As stated in the introduction, a power-law decay of the return amplitude is the hallmark of the OC [1, 2, 28].

The typical behavior of the return amplitude is shown in Fig. 1. Our numerical computations show that after an initial transient, $|\mathcal{L}(t)|$ displays two qualitatively different behaviors, and that we can go from one to the other by tuning the density. Above half filling, the return amplitude is well described by a power-law, while below it acquires an exponential decay. Notice that the lack of symmetry with respect to half-filling is to be expected, as the dynamics Eq. (1) explicitly breaks particle-hole symmetry: loosely speaking, the exchange $c_j \leftrightarrow (-1)^j c_j^\dagger$ leaves the Hamiltonian invariant while changing the sign of γ [42]. As a consequence, we will show only data for $\gamma > 0$, as those for $\gamma < 0$ (for the case of post-selection for $n_0 = 1$) can be obtained from the correspondence $\bar{n}(\gamma < 0) = 1 - \bar{n}(\gamma > 0)$.

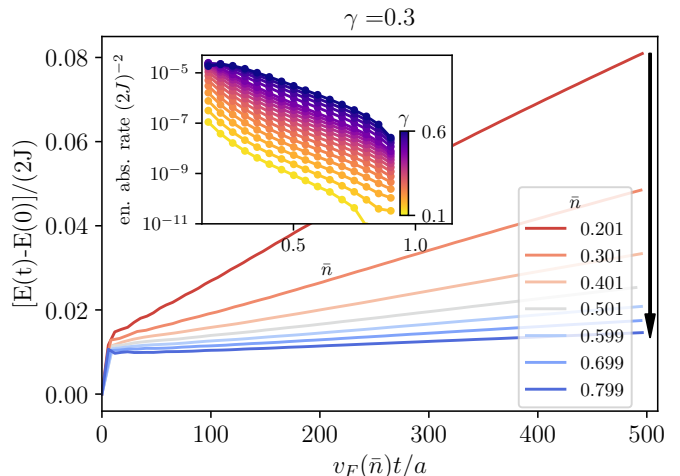


FIG. 2. Energy absorption as a function of the rescaled time for $L = 1000$, $J = 0.5$, $\gamma = 0.3$ and various densities. A monotonic behavior as a function of the density can be observed in the rate of energy absorption after a transient, which decreases upon increasing the density, as emphasized by the arrow on the right of the figure. Inset: density dependence of the energy absorption rate computed from a linear fit, at various values of γ . The rate decays exponentially with \bar{n} .

We fit $|\mathcal{L}(t)|$ assuming that after the transient it has the form $|\mathcal{L}(t)| = At^{-\beta}e^{-\Gamma t}$. The combined algebraic and exponential decay (besides being justified by the shape of the curves that we obtain) reflects the two processes that we expect to occur: the first is the OC behavior, while the latter can be interpreted as a sign of irreversible dynamics caused by the measurement process. This shape of $|\mathcal{L}(t)|$ is valid for $0.1 \lesssim \bar{n} \lesssim 0.9$ and $\gamma \lesssim J$: outside this range of parameters, the return amplitude has a more complicated behavior.

The typical density dependence of the two parameters β (the OC exponent) and Γ (the decay rate) for a chain of $L = 1000$ sites is shown in the inset of Fig. 1. The two parameters behave very differently, especially at small measurement rate $\gamma \lesssim J$: while β is essentially particle-hole symmetric, Γ decreases monotonically (and exponentially) with the filling. We show in [42] that the behavior of the OC exponent β can be predicted with bosonization, which yields $\beta_b(\bar{n}) = \gamma^2 / [2\pi v_F(\bar{n})]^2$. This expression depends on the filling only through the Fermi velocity $v_F = 2J \sin(\pi\bar{n})$, which is particle-hole symmetric, in accord with the numerics [60]. However, the power-law behavior is all that bosonization predicts. Namely, the existence of a nonvanishing Γ lies beyond bosonization. A numerical fit suggests (cf. [42]) that for small γ the decay rate behaves as $\ln \Gamma \approx a(\gamma) - b\bar{n}/\gamma^y$, where $a(\gamma)$ is approximately linear in γ , $b > 0$ and $y \approx 1.4$. This result suggests that Γ is non-perturbative in the measurement rate γ .

A second observable that we consider is the kinetic energy absorbed as a function of time, $E(t) \equiv$

$\langle \psi(t) | H | \psi(t) \rangle$, whose variation with respect to the initial state is shown in Fig. 2 for a fixed γ at various fillings. This quantity shows a steep transient, after which it begins to grow linearly in time. The interesting behavior is the dependence of the slope of the linear growth (namely, the energy absorption rate) on the filling. The inset in Fig. 2 shows that the rate decreases exponentially with the fermion density. In the case of our model, bosonization would predict that the energy should saturate as a function of time, as in the Hermitian case. This behavior depends on the excitation of only low-energy modes, which are those captured by the TLL Hamiltonian. The absorption of energy in the non-Hermitian scenario signals the broken time-reversal symmetry—or irreversibility—of the dynamics of the measured system. Indeed, the state will eventually converge to the many-body eigenstate of K with the smallest imaginary part of the eigenvalue, although this happens at very late times [14, 55], much larger than L/v_F .

We would like to point out that the value of the measurement rate γ does not play an important role in our results, as in all the plots that we are showing it is smaller than the bandwidth $4J$. In this parameter regime, a larger γ determines a quantitative change of the various effects, while keeping the qualitative picture unchanged [61]. In the Hermitian OC scenario, the smallness of γ ensures the applicability of bosonization, but the power-law behavior is non-perturbative [1, 2, 36]. Our calculations show that for the non-Hermitian version of the OC, bosonization is not applicable even in such perturbative regime.

Physical mechanism.— As observed in the numerics, the predictions of bosonization are violated if the density is low enough. We stress that our TLL predictions involve no approximations beyond the linearization of the dispersion relation, since we bosonize the model in such a way [1, 2, 62] that a quadratic Hamiltonian is obtained, to which no nonlinear terms need to be added within the usual theory of TLL. The validity of the linearization of the spectrum around the Fermi points typically relies only on the smallness of γ and gives reliable results in the Hermitian case [1, 2, 29]. So, what goes wrong in the bosonization procedure? The answer can be found by computing the single-particle spectrum of the Hamiltonian K . As discussed in [42], we find that the imaginary part of the eigenvalues (i.e. the decay rates of the eigenstates) is mostly flat near the middle of the band (momentum close to $\pi/2$), while it has two peaks near the band edges. This contrasts with the bosonized Hamiltonian, which predicts the same decay rate for all states [63]. Therefore, bosonization is capable of describing the physics around the Fermi surface as long as the latter lies near the middle of the band (and this explains why it predicts the OC behavior correctly), but it cannot account for the nontrivial dynamics that occurs at

the edges of the band. Indeed, this picture is confirmed by the time evolution of the occupation number of the momentum modes: while the discontinuity of the Fermi surface remains intact, the decay peaks cause an extra depletion deep inside the Fermi sea. The breakdown of bosonization that we are proposing is unusual, since it does not come from properties of the band dispersion at intermediate energy (such as the curvature at the Fermi surface [23]), but rather it comes from the properties of the imaginary part of the spectrum—the eigenstates’ lifetimes.

The existence of this faster-decaying modes has been already noticed in Ref. [64], in which they appear as the ones most strongly scattered by the imaginary potential. The momenta at which the peaks occur are $\pm q^*$ and $\pm(\pi - q^*)$, where q^* is determined approximately [64] from the requirement that the group velocity of the fermions is equal to the strength of the imaginary potential, $2J \sin q^* = \gamma/2$. This observation implies that these “special” modes are a consequence of the curvature of the band dispersion. Indeed, if we start with a perfectly linear fermion dispersion (the so-called Tomonaga model), these modes disappear, and we find again that the various observables are in excellent agreement with the results from bosonization. Thus, the breakdown of bosonization at low densities is a curvature effect, albeit different from the usual beyond-TLL physics [23], since the latter involves only the curvature near the Fermi surface, whereas here we observe effects coming from the curvature at the band edges.

While the extra depletion of low-momentum (and low-energy) modes in favor of higher-momentum ones explains why the system absorbs energy, the role of the density in determining the behavior still needs to be addressed. There is a similarity with the situation of the Hermitian OC in the presence of a bound state, where a non-analytic dependence of $\mathcal{L}(t)$ on the density is found [65]. Indeed, the special modes are quasi-bound states.

We can have a partial understanding of the role played by the density by generalizing the results of Ref. [37] for the Hermitian OC to the present, non-Hermitian case. For long times with respect to some microscopic timescale (represented by the UV cutoff α), the un-renormalized return probability $\tilde{\mathcal{L}}(t) = \langle FS | e^{-iKt} | FS \rangle$ has the form:

$$\ln \tilde{\mathcal{L}}(t) \sim -i\Delta E t - \beta \ln(\alpha t), \quad (4)$$

and the coefficients ΔE and β are determined in a non-perturbative fashion by the energy-dependent scattering phase $\delta(\varepsilon)$ associated with K . The key novelty in our setup is that the scattering phase for the non-Hermitian Hamiltonian K is in general *complex* [66]. The OC exponent is $\beta = \delta^2(\varepsilon_F)/\pi^2$, which depends only on the scattering phase at the Fermi energy ε_F . If ε_F is not too close to the band edges we find $\delta(\varepsilon_F) \approx i\gamma/(2v_F)$, which gives β in accord with the bosonization result, although with an extra minus sign (this phenomenon

has been already noticed in [38]—the correct sign is obtained when $\tilde{\mathcal{L}}(t)$ is divided by the norm of the state). The most interesting part is the term linear in time, which is proportional to $\Delta E = -\int_{-2J}^{\varepsilon_F} d\varepsilon \delta(\varepsilon)/\pi$ (known as Fumi’s theorem [28, 37]). For an ordinary scattering problem, ΔE is the shift in the ground-state energy caused by the external potential, a quantity which is obviously non-universal and depending on the full dispersion, but that contributes only to an innocuous overall phase. However, in our model ΔE has an imaginary part, which means that it contributes to an exponential decay of $\tilde{\mathcal{L}}(t)$ with a decay constant that is sensitive to all occupied states—hence, with a nontrivial density dependence [42].

Conclusions.— From a fundamental point of view, our research unveils a novel mechanism for departures from bosonization. The mechanism is distinct from more traditional explanations rooted in the effects of band curvature of the dispersion relation [23], and in this regard it illustrates transparently the profound difference between unitary and dissipative systems when it comes to the breakdown of low-energy collective descriptions.

Upon initial examination [42], the Lindblad dynamics governed by localized noise dephasing, albeit featuring the same non-Hermitian Hamiltonian as this work, does not exhibit the same characteristic signatures of the measurement-induced dynamics that we found. This observation implies that quantum jumps may obscure the mechanism we have elucidated above. Unraveling these features and developing a simplified model for controlled breakdown of bosonization within Lindblad dynamics would represent a natural extension of our research.

Recently, measurement-induced phase transitions in low-dimensional fermionic systems have been captured using an effective bosonized description [17]. Our findings could serve as a promising starting point for extending this analysis to interacting fermions or quantum spin chains undergoing monitored dynamics. At variance with [17], one could wonder whether the universality classes of such dynamical transitions may change when the Luttinger Liquid becomes inapplicable and processes similar to those presented here come into play. Among all the possible ramifications of our work, this appears to us as one of the most promising.

Acknowledgments.— We wish to thank Z. Weinstein and S. Diehl for helpful discussions and for providing comments on early versions of the manuscript. M.S. is grateful to R. J. Valencia Tortora and especially to O. Chelpanova for many useful discussions. This work has been supported by the DFG through the grant HADEQUAM-MA7003/3-1. We gratefully acknowledge the computing time granted through the project “DysQCorr” on the Mogon II supercomputer of the Johannes Gutenberg University Mainz (hpc.uni-mainz.de), which is a member of the AHRP (Alliance for High Performance Computing in Rhineland Palatinate, www.ahrp.info), and the Gauss Alliance e.V.

www.ahrp.info), and the Gauss Alliance e.V.

-
- [1] T. Giamarchi, *Quantum Physics in One Dimension*, 1st ed. (Clarendon Press, Oxford, 2003).
 - [2] A. O. Gogolin, A. A. Nersisyan, and A. M. Tsvelik, *Bosonization and Strongly Correlated Systems* (Cambridge University Press, Cambridge, 1998).
 - [3] M. A. Cazalilla, Effect of suddenly turning on interactions in the Luttinger model, *Phys. Rev. Lett.* **97**, 156403 (2006).
 - [4] A. Iucci and M. A. Cazalilla, Quantum quench dynamics of the Luttinger model, *Phys. Rev. A* **80**, 063619 (2009).
 - [5] M. A. Cazalilla and M.-C. Chung, Quantum quenches in the Luttinger model and its close relatives, *J. Stat. Mech.* **2016**, 064004 (2016).
 - [6] J. Dziarmaga and M. Tylutki, Excitation energy after a smooth quench in a Luttinger liquid, *Phys. Rev. B* **84**, 214522 (2011).
 - [7] S. Ngo Dinh, D. A. Bagrets, and A. D. Mirlin, Interaction quench in nonequilibrium Luttinger liquids, *Phys. Rev. B* **88**, 245405 (2013).
 - [8] A. Iucci and M. A. Cazalilla, Quantum quench dynamics of the sine-gordon model in some solvable limits, *New Journal of Physics* **12**, 055019 (2010).
 - [9] M. Buchhold, M. Heyl, and S. Diehl, Prethermalization and thermalization of a quenched interacting Luttinger liquid, *Phys. Rev. A* **94**, 013601 (2016).
 - [10] E. Coira, F. Becca, and A. Parola, Quantum quenches in one-dimensional gapless systems, *Eur. Phys. J. B* **86**, 55 (2013).
 - [11] A. Bácsi and B. Dóra, Lindbladian route towards thermalization of a Luttinger liquid, *Phys. Rev. B* **107**, 125149 (2023).
 - [12] A. Bácsi, C. P. Moca, and B. Dóra, Dissipation-induced Luttinger liquid correlations in a one-dimensional fermi gas, *Phys. Rev. Lett.* **124**, 136401 (2020).
 - [13] M. Buchhold and S. Diehl, Nonequilibrium universality in the heating dynamics of interacting Luttinger liquids, *Phys. Rev. A* **92**, 013603 (2015).
 - [14] H. Fröml, C. Muckel, C. Kollath, A. Chiocchetta, and S. Diehl, Ultracold quantum wires with localized losses: Many-body quantum zeno effect, *Phys. Rev. B* **101**, 144301 (2020).
 - [15] A. Bácsi, C. P. Moca, G. Zaránd, and B. Dóra, Vaporization dynamics of a dissipative quantum liquid, *Phys. Rev. Lett.* **125**, 266803 (2020).
 - [16] S. J. Garratt, Z. Weinstein, and E. Altman, Measurements conspire nonlocally to restructure critical quantum states (2022), [arXiv:2207.09476 \[cond-mat.stat-mech\]](https://arxiv.org/abs/2207.09476).
 - [17] M. Buchhold, Y. Minoguchi, A. Altland, and S. Diehl, Effective theory for the measurement-induced phase transition of Dirac fermions, *Physical Review X* **11** (2021).
 - [18] B. Ladewig, S. Diehl, and M. Buchhold, Monitored open fermion dynamics: Exploring the interplay of measurement, decoherence, and free Hamiltonian evolution, *Phys. Rev. Res.* **4**, 033001 (2022).
 - [19] M. Collura, P. Calabrese, and F. H. L. Essler, Quantum quench within the gapless phase of the spin $- \frac{1}{2}$ Heisen-

- berg XXZ spin chain, *Phys. Rev. B* **92**, 125131 (2015).
- [20] F. Pollmann, M. Haque, and B. Dóra, Linear quantum quench in the Heisenberg XXZ chain: Time-dependent Luttinger-model description of a lattice system, *Phys. Rev. B* **87**, 041109 (2013).
- [21] C. Karrasch, J. Rentrop, D. Schuricht, and V. Meden, Luttinger-liquid universality in the time evolution after an interaction quench, *Phys. Rev. Lett.* **109**, 126406 (2012).
- [22] D. M. Kennes and V. Meden, Luttinger liquid properties of the steady state after a quantum quench, *Phys. Rev. B* **88**, 165131 (2013).
- [23] A. Imambekov, T. L. Schmidt, and L. I. Glazman, One-dimensional quantum liquids: Beyond the Luttinger liquid paradigm, *Rev. Mod. Phys.* **84**, 1253 (2012).
- [24] D. B. Gutman, Y. Gefen, and A. D. Mirlin, Nonequilibrium Luttinger liquid: Zero-bias anomaly and dephasing, *Phys. Rev. Lett.* **101**, 126802 (2008).
- [25] D. B. Gutman, Y. Gefen, and A. D. Mirlin, Bosonization of one-dimensional fermions out of equilibrium, *Phys. Rev. B* **81**, 085436 (2010).
- [26] D. B. Gutman, Y. Gefen, and A. D. Mirlin, Full counting statistics of a Luttinger liquid conductor, *Phys. Rev. Lett.* **105**, 256802 (2010).
- [27] P. W. Anderson, Infrared catastrophe in fermi gases with local scattering potentials, *Phys. Rev. Lett.* **18**, 1049 (1967).
- [28] G. D. Mahan, *Many-Particle Physics*, 2nd ed. (Plenum press, New York, 1993).
- [29] K. D. Schotte and U. Schotte, Tomonaga's model and the threshold singularity of X-ray spectra of metals, *Phys. Rev.* **182**, 479 (1969).
- [30] A. C. Hewson, *The Kondo Problem to Heavy Fermions*, Cambridge Studies in Magnetism (Cambridge University Press, 1993).
- [31] M. Heyl and S. Kehrein, X-ray edge singularity in optical spectra of quantum dots, *Phys. Rev. B* **85**, 155413 (2012).
- [32] N. d'Ambrumenil and B. Muzykantskii, Fermi gas response to time-dependent perturbations, *Phys. Rev. B* **71**, 045326 (2005).
- [33] F. Grusdt, K. Seetharam, Y. Shchadilova, and E. Demler, Strong-coupling bose polarons out of equilibrium: Dynamical renormalization-group approach, *Phys. Rev. A* **97**, 033612 (2018).
- [34] M. Knap, A. Shashi, Y. Nishida, A. Imambekov, D. A. Abanin, and E. Demler, Time-dependent impurity in ultracold fermions: Orthogonality catastrophe and beyond, *Phys. Rev. X* **2**, 041020 (2012).
- [35] A. Shashi, F. Grusdt, D. A. Abanin, and E. Demler, Radio-frequency spectroscopy of polarons in ultracold bose gases, *Phys. Rev. A* **89**, 053617 (2014).
- [36] P. Nozières and C. T. De Dominicis, Singularities in the X-ray absorption and emission of metals. iii. one-body theory exact solution, *Phys. Rev.* **178**, 1097 (1969).
- [37] M. Combescot and P. Nozières, Infrared catastrophe and excitons in the X-ray spectra of metals, *J. Phys. (France)* **32**, 913 (1971).
- [38] F. Tonielli, R. Fazio, S. Diehl, and J. Marino, Orthogonality catastrophe in dissipative quantum many-body systems, *Phys. Rev. Lett.* **122**, 040604 (2019).
- [39] C. Lupo and M. Schiró, Transient Loschmidt echo in quenched Ising chains, *Phys. Rev. B* **94**, 014310 (2016).
- [40] M. Schiró and A. Mitra, Transient orthogonality catastrophe in a time-dependent nonequilibrium environment, *Phys. Rev. Lett.* **112**, 246401 (2014).
- [41] W. Berdanier, J. Marino, and E. Altman, Universal dynamics of stochastically driven quantum impurities, *Phys. Rev. Lett.* **123**, 230604 (2019).
- [42] See the Supplementary Material for technical details.
- [43] H. M. Wiseman and G. J. Milburn, *Quantum Measurement and Control* (Cambridge University Press, Cambridge, 2009).
- [44] M. A. Nielsen and I. L. Chuang, *Quantum Computation and Quantum Information: 10th Anniversary Edition* (Cambridge University Press, Cambridge, 2010).
- [45] X. Turkeshi and M. Schiró, Entanglement and correlation spreading in non-Hermitian spin chains, *Phys. Rev. B* **107**, L020403 (2023).
- [46] Y. Le Gal, X. Turkeshi, and M. Schiró, Volume-to-area law entanglement transition in a non-Hermitian free fermionic chain, *SciPost Phys.* **14**, 138 (2023).
- [47] X. Turkeshi, A. Biella, R. Fazio, M. Dalmonte, and M. Schiró, Measurement-induced entanglement transitions in the quantum Ising chain: From infinite to zero clicks, *Phys. Rev. B* **103**, 224210 (2021).
- [48] A. J. Daley, Quantum trajectories and open many-body quantum systems, *Advances in Physics* **63**, 77 (2014).
- [49] H. F. Fröml, *Localized dissipation in fermionic quantum wires*, Ph.D. thesis, Universität zu Köln (2020).
- [50] H. Fröml, A. Chiocchetta, C. Kollath, and S. Diehl, Fluctuation-induced quantum zeno effect, *Phys. Rev. Lett.* **122**, 040402 (2019).
- [51] T. Müller, M. Gievers, H. Fröml, S. Diehl, and A. Chiocchetta, Shape effects of localized losses in quantum wires: Dissipative resonances and nonequilibrium universality, *Phys. Rev. B* **104**, 155431 (2021).
- [52] M. Foss-Feig, A. J. Daley, J. K. Thompson, and A. M. Rey, Steady-state many-body entanglement of hot reactive fermions, *Phys. Rev. Lett.* **109**, 230501 (2012).
- [53] M. Naghiloo, M. Abbasi, Y. N. Joglekar, and K. W. Murch, Quantum state tomography across the exceptional point in a single dissipative qubit, *Nature Physics* **15**, 1232 (2019).
- [54] P. L. Krapivsky, K. Mallick, and D. Sels, Free fermions with a localized source, *J. Stat. Mech.* , 113108 (2019).
- [55] P. E. Dolgirev, J. Marino, D. Sels, and E. Demler, Non-gaussian correlations imprinted by local dephasing in fermionic wires, *Phys. Rev. B* **102**, 100301 (2020).
- [56] B. Yan, S. A. Moses, B. Gadway, J. P. Covey, K. R. A. Hazzard, A. M. Rey, D. S. Jin, and J. Ye, Observation of dipolar spin-exchange interactions with lattice-confined polar molecules, *Nature* **501**, 521 (2013).
- [57] B. Zhu, B. Gadway, M. Foss-Feig, J. Schachenmayer, M. L. Wall, K. R. A. Hazzard, B. Yan, S. A. Moses, J. P. Covey, D. S. Jin, J. Ye, M. Holland, and A. M. Rey, Suppressing the loss of ultracold molecules via the continuous quantum zeno effect, *Phys. Rev. Lett.* **112**, 070404 (2014).
- [58] K. Sponselee, L. Freystatzky, B. Abeln, M. Diem, B. Hundt, A. Kochanke, T. Ponath, B. Santra, L. Mathay, K. Sengstock, and C. Becker, Dynamics of ultracold quantum gases in the dissipative fermi-hubbard model, *Quantum Sci. Technol.* **4**, 014002 (2018).
- [59] X. Cao, A. Tilloy, and A. D. Luca, Entanglement in a fermion chain under continuous monitoring, *SciPost Phys.* **7**, 024 (2019).
- [60] The disagreement of the fitted exponent with respect to β_b at larger γ can be attributed to the local curvature

of the dispersion around the Fermi energy, just as in the Hermitian case [1, 2].

- [61] Unless the density is too low or too high, so that the Fermi momentum crosses the “special momenta” q^* reported in the following Section. There are also qualitative changes in the nonperturbative regime $\gamma > 4J$ caused by the crossing of an exceptional point [49, 64], not treated here.
- [62] C. L. Kane, K. A. Matveev, and L. I. Glazman, Fermi-edge singularities and backscattering in a weakly interacting one-dimensional electron gas, *Phys. Rev. B* **49**, 2253 (1994).
- [63] Indeed, it differs from a \mathcal{PT} -symmetric [67] Hamiltonian by an imaginary constant only, which is unobservable in the nonlinear dynamics Eq. (1).
- [64] P. C. Burke, J. Wiersig, and M. Haque, Non-Hermitian scattering on a tight-binding lattice, *Phys. Rev. A* **102**, 012212 (2020).
- [65] A. M. Zagoskin and I. Affleck, Fermi edge singularities: Bound states and finite-size effects, *J. Phys. A: Math. Gen.* **30**, 5743 (1997).
- [66] This behavior of the scattering phase out of equilibrium has been associated to irreversibility [68].
- [67] Y. Ashida, Z. Gong, and M. Ueda, Non-Hermitian physics, *Advances in Physics* **69**, 249 (2020).
- [68] T.-K. Ng, X-ray-edge singularity in nonequilibrium systems, *Phys. Rev. B* **51**, 2009 (1995).

Supplemental material – Orthogonality catastrophe beyond Luttinger liquid from post-selection

Martino Stefanini and Jamir Marino

Institut für Physik, Johannes Gutenberg-Universität Mainz, D-55099 Mainz, Deutschland

(Dated: October 3, 2023)

REALIZATION OF THE DYNAMICS

As mentioned in the main text, there are two main approaches for reproducing the nonlinear Schrödinger equation

$$i \frac{d}{dt} |\psi(t)\rangle = \left[H - i \frac{\gamma}{2} n_0 + i \frac{\gamma}{2} \langle \psi(t) | n_0 | \psi(t) \rangle \right] |\psi(t)\rangle \quad (1)$$

that governs the dynamics of the non-Hermitian orthogonality catastrophe (OC). The first approach is to perform a series of weak measurements chosen such that the set of Kraus operators [1] that describe the measurements includes the desired one,

$$M \propto e^{-\frac{\gamma \delta t}{2} n_0} . \quad (2)$$

The state of the system will evolve stochastically, as a function of the random measurement outcomes, and the desired dynamics (1) will be obtained by post-selecting the state trajectories for which the outcomes correspond to (2). This strategy is known as "no-click" scenario [2–5]. A possible choice (in the $\delta t \rightarrow 0$ limit) is given by the set

$$\begin{cases} M_0(\delta t) = e^{-\frac{\gamma \delta t}{2} n_0} \\ M_1(\delta t) = (\gamma \delta t)^{1/2} n_0 \end{cases} , \quad (3)$$

with outcomes labeled as 0 and 1, which correspond to finding no fermions or one fermion at the measured site, respectively. This setup is slightly less general than the model considered in the main text as it requires $\gamma > 0$.

The second approach uses a suitable dissipative (Lindbladian) dynamics to "reconstruct" Eq. (1). As mentioned in the main text, one should choose a dissipative dynamics

$$\frac{d}{dt} \rho(t) = -i[H, \rho] + \gamma \left(\mathcal{J} \rho \mathcal{J}^\dagger - \frac{1}{2} \{ \mathcal{J}^\dagger \mathcal{J}, \rho \} \right) \quad (4)$$

such that the jump operator \mathcal{J} satisfies $\mathcal{J}^\dagger \mathcal{J} = n_0$, so that the non-Hermitian part of the Lindbladian reproduces the non-Hermitian OC Hamiltonian $H - i \frac{\gamma}{2} \mathcal{J}^\dagger \mathcal{J} = H - i \frac{\gamma}{2} n_0 = K$. Suitable jump operators are the ones that describe localized single particle loss $\mathcal{J} = c_{j_0}$ [6–9], localized single particle gain $\mathcal{J} = c_{j_0}^\dagger$ [10] and localized dephasing $\mathcal{J} = n_0$ [11, 12]. The first two cases are the most promising: for each time t , the system is let to evolve from the same initial state $|FS\rangle$ and at the end of the dynamics the total number of particles is counted, and if the number has changed from the initial value, the run is discarded. The average values of other observables that are measured on the remaining set of runs would correspond to the ones calculated from the state $|\tilde{\psi}(t)\rangle = e^{-iKt} |FS\rangle$. The expectation values of the nonlinear dynamics of Eq. (1) are then obtained dividing by the normalization $\langle \tilde{\psi}(t) | \tilde{\psi}(t) \rangle$, which is the probability of not altering the number of particles, i.e. the success rate of the runs.

We notice that the dephasing case $\mathcal{J} = n_0$ is not suitable for the procedure outlined above, since there is no way to reconstruct *a posteriori* whether a dissipative event (a jump) has occurred. The only way to proceed would be to fall back to the continuous monitoring of Eq. (3), which is indeed a stochastic unraveling of a Lindblad equation with local dephasing.

We notice that the dissipative strategy outlined above does not simply reduce to the one based on measurements: at a given time t one generally has to measure a global observable (in our case, the total number of fermions) *once*, and then perform a post-selection based on the result, whereas the first strategy requires the recording a local observable (the outcome of the density measurement) for each instant before t .

A different way to use a dissipative dynamics to reconstruct Eq. (1) is to introduce an "impurity" in the system, which triggers the dynamics and serves as a probe of the rest of the system, in analogy with the usual OC case [13–16]. In more detail, we assume that at the measured site j_0 it is possible to introduce an immobile impurity d , that can interact with a "bath" fermion c_{j_0} at the site so that both fermions are then lost from the system.

This type of two-body loss can be realized with ultra-cold atoms [17–19]. The Lindblad equation for the combined impurity-bath system is then Eq. (4) with $\mathcal{J} = d c_{j_0}$. The non-Hermitian generator of the Lindbladian dynamics is $\tilde{H} = H - i\gamma/2 d^\dagger d n_0$, from which we see that the presence of the impurity ($d^\dagger d = 1$) induces the desired non-Hermitian dynamics (1) with $\tilde{H} = H - i\gamma/2 n_0 \equiv K$. Not only the impurity degree of freedom serves as a switch of the imaginary potential, but it can also be used as a probe to extract the full return amplitude of the non-Hermitian dynamics of the bath. This can be obtained by choosing the initial impurity state in a superposition of occupied ($|1\rangle$) and empty ($|0\rangle$).

We can decompose the density matrix as $\rho(t) = \sum_{\alpha,\beta \in \{0,1\}} R_{\alpha\beta}(t) |\alpha\rangle\langle\beta|$, where $\{|0\rangle, |1\rangle\}$ form the basis of the impurity states and $R_{\alpha\beta}(t)$ are operators acting on the c fermions' Hilbert space. Since $\rho(t)$ is Hermitian, we have $R_{\alpha\alpha}^\dagger = R_{\alpha\alpha}$ and $R_{10}^\dagger = R_{01}$. Plugging this decomposition in the Lindblad equation we find that the R operators satisfy

$$\begin{aligned} \frac{d}{dt} R_{00}(t) &= -i[H, R_{00}(t)] + \gamma c_{j_0} R_{11}(t) c_{j_0}^\dagger, \\ \frac{d}{dt} R_{10}(t) &= -iK R_{10}(t) + iR_{10}(t)H, \\ \frac{d}{dt} R_{11}(t) &= -iK R_{11}(t) + iR_{11}(t)K^\dagger, \end{aligned} \quad (5)$$

that are solved by

$$\begin{aligned} R_{00}(t) &= e^{-iHt} R_{00}(0) e^{iHt} + \gamma \int_0^t ds e^{-iH(t-s)} c_{j_0} R_{11}(s) c_{j_0}^\dagger e^{iH(t-s)}, \\ R_{10}(t) &= e^{-iKt} R_{10}(0) e^{iHt}, \\ R_{11}(t) &= e^{-iKt} R_{11}(0) e^{iK^\dagger t}. \end{aligned} \quad (6)$$

Let us assume that the impurity and bath are initially prepared in uncorrelated pure states $\rho(0) = |FS\rangle_c \langle FS| \otimes |\varphi\rangle\langle\varphi|$, where $|FS\rangle_c$ is the ground state of the bath and $|\varphi\rangle = \sum_{\alpha=0}^1 \varphi_\alpha |\alpha\rangle$ is a generic state of the impurity. Then $R_{\alpha\beta}(0) = \varphi_\alpha \varphi_\beta^* |FS\rangle_c \langle FS|$ and Eqs. (6) yield

$$\begin{aligned} R_{00}(t) &= |\varphi_0|^2 |FS\rangle_c \langle FS| + |\varphi_1|^2 \gamma \int_0^t ds e^{-iH(t-s)} c_{j_0} |\tilde{\psi}(s)\rangle_c \langle \tilde{\psi}(s)| c_{j_0}^\dagger e^{iH(t-s)}, \\ R_{10}(t) &= \varphi_1 \varphi_0^* |\tilde{\psi}(t)\rangle_c \langle FS| e^{iE_{FS}t}, \\ R_{11}(t) &= |\varphi_1|^2 |\tilde{\psi}(t)\rangle_c \langle \tilde{\psi}(t)|, \end{aligned} \quad (7)$$

in which we introduced the ground-state energy of the bath $E_{FS} \equiv \langle FS|H|FS\rangle$ and the un-normalized state $|\tilde{\psi}(t)\rangle \equiv e^{-iKt} |FS\rangle$. Already at this level, we observe that the desired non-Hermitian dynamics is contained in the full state of the system. Actually, in order to extract the return amplitude $\mathcal{L}(t) \equiv {}_c \langle FS|\tilde{\psi}(t)\rangle_c / {}_c \langle \tilde{\psi}(t)|\tilde{\psi}(t)\rangle_c^{1/2}$ only the density matrix ρ^d of the impurity is needed. Indeed, from $\rho_{\alpha\beta}^d(t) \equiv \text{Tr}_c R_{\alpha\beta}(t)$ we obtain:

$$\rho^d(t) = \begin{pmatrix} 1 - |\varphi_1|^2 \langle \tilde{\psi}(t)|\tilde{\psi}(t)\rangle & \varphi_0 \varphi_1^* {}_c \tilde{\mathcal{L}}^*(t) e^{-iE_{FS}t} \\ \varphi_1 \varphi_0^* \tilde{\mathcal{L}}(t) e^{iE_{FS}t} & |\varphi_1|^2 \langle \tilde{\psi}(t)|\tilde{\psi}(t)\rangle \end{pmatrix}, \quad (8)$$

where $\tilde{\mathcal{L}}(t) \equiv {}_c \langle FS|\tilde{\psi}(t)\rangle_c$, and the ρ_{00}^d element has been simplified using the property

$$\langle \tilde{\psi}(t)|\tilde{\psi}(t)\rangle = 1 - \gamma \int_0^t ds \langle \tilde{\psi}(t)|n_0|\tilde{\psi}(t)\rangle,$$

that can be proven from $i d/dt |\tilde{\psi}(t)\rangle = K|\tilde{\psi}(t)\rangle$. Thus, a measurement of the impurity population gives access to the norm ${}_c \langle \tilde{\psi}(t)|\tilde{\psi}(t)\rangle_c$, while the off-diagonal elements of ρ_d give the overlap ${}_c \langle FS|\tilde{\psi}(t)\rangle_c$. One can also employ a Ramsey interferometry scheme [16] to measure ${}_c \langle FS|\tilde{\psi}(t)\rangle_c$ from the impurity population after the application of a $\pi/2$ -pulse.

Concluding this Section, we remark that all the approaches presented incur in some form of post-selection problem, since in all cases a fraction of the experimental runs has to be discarded, and in general this fraction increases exponentially on a timescale $(\bar{n}\gamma)^{-1}$. However, this does not necessarily preclude the possibility to observe the phenomena reported in the main text, because it may still be possible to find a regime of density and measurement rate in which they are visible before the post-selection overhead becomes too large. The exact determination of the extent of this regime requires will not be pursued further.

PARTICLE-HOLE TRANSFORMATION

Let us introduce the basis of the fermionic Fock space for spinless fermions moving on a 1D lattice of L sites as $|\mathbf{n}\rangle$, where \mathbf{n} is a string of 0s and 1s enumerating the occupation of the lattice sites $j = 0 \dots L-1$. The length of \mathbf{n} is L . In other words, $\mathbf{n} = |n_0 \dots n_{L-1}\rangle \equiv (c_0^\dagger)^{n_0} \dots (c_{L-1}^\dagger)^{n_{L-1}} |0\rangle$, where $|0\rangle = |\mathbf{0}\rangle = |0 \dots 0\rangle$ is the vacuum. We choose to order the application of the fermion creation operators as the order of the sites, but the choice of this convention does not change the results. Then, the particle-hole (ph) transformation is implemented by the operator $\mathcal{C} = \mathcal{S}\mathcal{P}$, where

$$\mathcal{S} \equiv e^{i\pi \sum_j c_j^\dagger c_j} , \quad (9a)$$

$$\mathcal{P} \equiv \sum_{\mathbf{n}} |\text{NOT}(\mathbf{n})\rangle \langle \mathbf{n}| , \quad (9b)$$

in which NOT is the logical NOT operation that swaps the values of 0 and 1 in the strings. Both the above operators are self-adjoint and square to the identity. The two operators commute if the number of sites is even, and anticommute otherwise: since $\mathcal{S}\mathcal{P} = (-1)^L \mathcal{P}\mathcal{S}$. The operator $\mathcal{C}' = \mathcal{P}\mathcal{S}$ would be equally good as a ph transformation.

The action of \mathcal{P} is evident: it changes every occupied site (particle) to an empty site (hole), and vice-versa. It induces the following transformation on the fermionic operators:

$$\begin{aligned} \mathcal{P}c_j\mathcal{P}^\dagger &= \sum_{\mathbf{n}, \mathbf{m}} |\text{NOT}(\mathbf{m})\rangle \langle \mathbf{m}| c_j |\mathbf{n}\rangle \langle \text{NOT}(\mathbf{n})| = \sum_{\mathbf{n}, \mathbf{m} | n_j=1} |\text{NOT}(\mathbf{m})\rangle \delta_{\mathbf{m}, \mathbf{n} - (1)_j} (-1)^{\sum_{k<j} n_k} \langle \text{NOT}(\mathbf{n})| = \\ &= \sum_{\mathbf{n} | n_j=0} (-1)^{\sum_{k<j} (1-n_k)} |\mathbf{n} + (1)_j\rangle \langle \mathbf{n}| = c_j^\dagger \sum_{\mathbf{n}} (-1)^{\sum_{k<j} 1} |\mathbf{n}\rangle \langle \mathbf{n}| = (-1)^{j-1} c_j^\dagger , \end{aligned} \quad (10)$$

where the notation $|\mathbf{n} \pm (1)_j\rangle$ stands for $|n_0 \dots n_j \pm 1 \dots n_{L-1}\rangle$, and we have used

$$\begin{aligned} c_j |\mathbf{n}\rangle &= \delta_{n_j, 1} (-1)^{\sum_{k<j} n_k} |\mathbf{n} - (1)_j\rangle \\ c_j^\dagger |\mathbf{n}\rangle &= \delta_{n_j, 0} (-1)^{\sum_{k<j} n_k} |\mathbf{n} + (1)_j\rangle \end{aligned} \quad (11)$$

The action of \mathcal{S} adds minus sign $\mathcal{S}c_j\mathcal{S}^\dagger = -c_j$, so that the full particle-hole transformation of the fermion operators has the usual form: $\mathcal{C}c_j\mathcal{C}^\dagger = (-1)^j c_j^\dagger$. In momentum space, this transformation reads

$$\mathcal{C}c_p\mathcal{C}^\dagger = c_{-p-\pi}^\dagger = \begin{cases} c_{\pi-p}^\dagger & \text{for } p \in [0, \pi] \\ c_{3\pi-p}^\dagger & \text{for } p \in]\pi, 2\pi[\end{cases} . \quad (12)$$

We can now see how this transformation acts on the nonlinear Schrödinger equation (1) that governs the post-selected dynamics. Its solution can be obtained as $|\psi(t)\rangle = |\tilde{\psi}(t)\rangle / \langle \tilde{\psi}(t) | \tilde{\psi}(t) \rangle^{1/2}$, where $|\tilde{\psi}(t)\rangle = e^{-iKt} |\psi(0)\rangle$. Suppose that we start from the state $|\psi^{\mathcal{C}}(0)\rangle = \mathcal{C}|\psi(0)\rangle$. If $|\psi(0)\rangle$ has a fixed number of fermions N_f , then the new state has the “dual” number of fermions $N_f^{\mathcal{C}} = L - N_f$. Then

$$|\tilde{\psi}^{\mathcal{C}}(t)\rangle = \mathcal{C}e^{-i\mathcal{C}K\mathcal{C}t} |\psi(0)\rangle = e^{-\gamma t/2} \mathcal{C}e^{-iK^\dagger t} |\psi(0)\rangle ,$$

since $\mathcal{C}(H - i\gamma/2 n_0)\mathcal{C} = H + i\gamma/2 n_0 - i\gamma/2 = K^\dagger - i\gamma/2$. The normalized state is therefore

$$|\psi^{\mathcal{C}}(t)\rangle = \frac{\mathcal{C}e^{-iK^\dagger t} |\psi(0)\rangle}{\langle \psi(0) | e^{iKt} e^{-iK^\dagger t} | \psi(0) \rangle^{1/2}} = \mathcal{C} |\psi_{-\gamma}(t)\rangle ,$$

which implies that the $|\psi^{\mathcal{C}}(t)\rangle$ is the ph-transformed solution $|\psi_{-\gamma}(t)\rangle$ of the nonlinear Schrödinger equation with $\gamma \rightarrow -\gamma$:

$$i \frac{d}{dt} |\psi_{-\gamma}(t)\rangle = \left[K^\dagger - i \frac{\gamma}{2} \langle \psi_{-\gamma}(t) | n_0 | \psi_{-\gamma}(t) \rangle \right] |\psi_{-\gamma}(t)\rangle$$

and initial condition $|\psi_{-\gamma}(0)\rangle = |\psi(0)\rangle$. This completes the proof of our claim that the post-selected dynamics is not symmetric under a ph transformation, and that such a ph transformation is equivalent to a change of sign of γ . This would be also valid for a Hermitian impurity, $H_V = H + Vn_0$. Indeed, the $V < 0$ scenario features a bound state

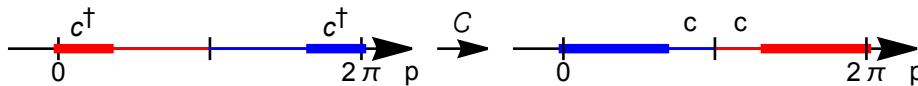


FIG. 1. Action of the particle-hole transformation on the Fermi sea. Thick and thin lines correspond to occupied and empty states, respectively. Notice that the order of the states is also reversed by \mathcal{C} .

[13] that is absent from the $V > 0$ situation (in which there is actually an anti-bound state). As a consequence of the results above, we have that

$$\mathcal{L}^{\mathcal{C}}(t) \equiv \langle \psi^{\mathcal{C}}(0) | \psi^{\mathcal{C}}(t) \rangle = \langle \psi_{-\gamma}(0) | \psi_{-\gamma}(t) \rangle$$

and

$$E^{\mathcal{C}}(t) \equiv \langle \psi^{\mathcal{C}}(t) | H | \psi^{\mathcal{C}}(t) \rangle = \langle \psi_{-\gamma}(t) | H | \psi_{-\gamma}(t) \rangle,$$

showing the absence of ph symmetry in these quantities and the property that their behavior starting from the ph conjugate state $|\psi^{\mathcal{C}}(0)\rangle = \mathcal{C}|\psi(0)\rangle$ is equivalent to the behavior of the solution with the original initial state but with the opposite sign of γ .

In all our simulations, the initial state is the Fermi sea $|FS\rangle$. In the main text we claimed that the observables that we measure for a certain γ and filling $\bar{n} = N_f/L$ are the same as those for $-\gamma$ and filling $\bar{n}^{\mathcal{C}} = 1 - \bar{n}$. This can be seen by proving that $\mathcal{C}|FS\rangle$ is the Fermi sea with the complementary filling $1 - \bar{n}$. As shown graphically in Fig. 1 using Eq. (12), this is exactly what happens.

DETAILS OF NUMERICAL IMPLEMENTATION

Numerical algorithm

We repeat here the numerical method that we employed to compute the dynamics, taken from Ref. [20]. A general Gaussian pure state can be written as

$$|\psi\rangle = \prod_{i=1}^{N_f} \sum_{j=0}^{L-1} U_{ji} c_j^\dagger |0\rangle, \quad (13)$$

where $|0\rangle$ is the fermionic vacuum and U_{ji} is simply the collection of the single-particle wave functions. The time evolution generated by a quadratic Hamiltonian [such as our nonlinear Schrödinger equation (1)] will conserve the above form of the state, since it will transform the c_j s linearly according to the single-particle Hamiltonian: $e^{-i\sum_{ii'} h_{ii'} c_i^\dagger c_{i'} t} c_j^\dagger e^{i\sum_{ii'} h_{ii'} c_i^\dagger c_{i'} t} = \sum_{j'} (e^{-iht})_{jj'} c_{j'}^\dagger$. The result is that we only need to compute the single-particle time evolution operator e^{-iht} to evolve U : $\tilde{U}(t + \delta t) = e^{-ih\delta t} U(t)$. The normalization of the state requires that U is an isometry, $U^\dagger(t)U(t) = \mathbb{1}_{N_f}$. This requirement can be imposed at each time step by a QR decomposition, $\tilde{U}(t + \delta t) = QR$, and setting the new U matrix to $U(t + \delta t) = Q$. A useful by-product of this method is that the correlation function of the fermions is easily computed from U : $\langle c_i^\dagger c_j \rangle = (UU^\dagger)_{ij}$.

In our case, the U matrix reads $U_{ji}(t) = \phi_{p_i}(j, t)$, where the p_i s run over the initial occupied momentum states. The wave functions obey the initial condition $\phi_{p_i}(j, t=0) = e^{ip_i j}/L^{1/2}$, and the time evolution is conveniently Trotterized as $e^{-i\kappa\delta t} \approx e^{-ih\delta t/2} e^{-\gamma/2n\delta t} e^{-ih\delta t/2}$, where κ , h and n are the single-particle versions of K , H and n_0 , respectively. The unitary part, $e^{-ih\delta t/2}$, can be easily computed in the momentum basis where it is diagonal, while $e^{-\gamma/2n\delta t}$ is diagonal in real space. Different time steps δt have been taken in the interval $\delta t = 0.01$ to 0.04 (in the units where $2J = 1$) to verify convergence. In particular, the data for $L = 1000$ are for $\delta t = 0.04$.

Fits of return amplitude

As stated in the main text, we assume that the return amplitude has the long-time profile $|\mathcal{L}(t)| = At^{-\beta}e^{-\Gamma t}$. To find the values of A , β and Γ we have performed a numerical fit of $\ln|\mathcal{L}(t)|$ to $\ln A - \beta \ln t - \Gamma t$ using a simple

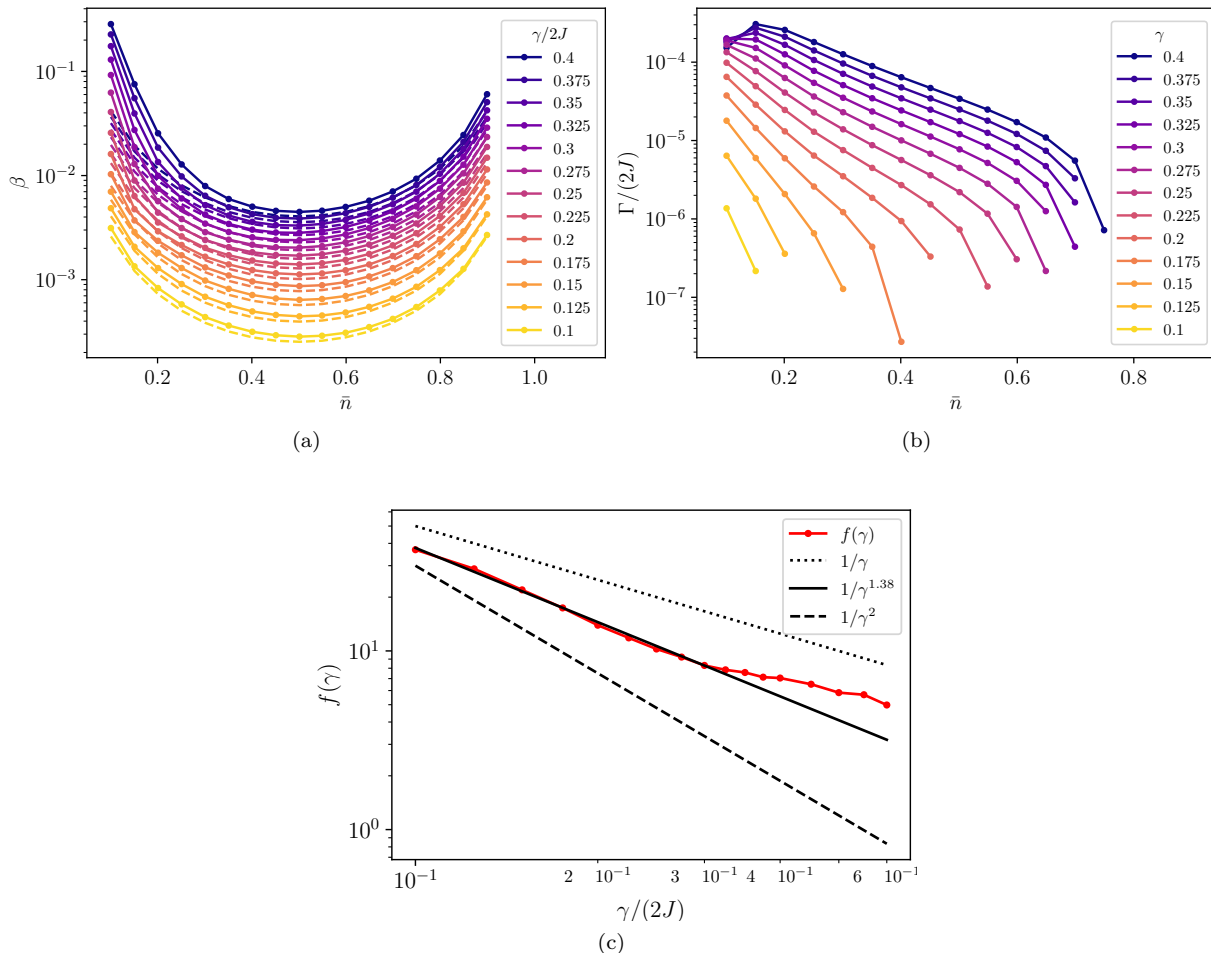


FIG. 2. Parameters fitted from the return amplitude. (a) The OC parameter β , compared with the bosonization prediction (dashed lines). (b) The exponential decay rate Γ . (c) The fitted dependence of Γ on the density, $\ln \Gamma = a(\gamma) - f(\gamma)\bar{n}$, showing the probable power-law increase of $f(\gamma)$ at small γ and hence the nonperturbative nature of Γ .

least-squares minimization. The results are shown in Figs. 2a and 2b. The uncertainty on the fitted parameters is computed as $\delta a_j = [\chi^2(Q^{-1})_{jj}/(N-3)]^{1/2}$, where $\mathbf{a} = (A, \beta, \Gamma)$, $\chi^2 = \sum_i (\ln |\mathcal{L}(t_i)| - \ln A + \beta \ln t_i + \Gamma t_i)^2$ is the sum of the squared residuals, N is the number of data, and $Q = M^T M$, in which M is defined by $M_{i1} = 1$, $M_{i2} = \ln t_i$ and $M_{i3} = t_i$. The uncertainties computed in this way are always smaller than the plotted points themselves.

The meaning of the behavior of β and Γ as a function of the density has been discussed at length in the main text. Here we just notice that if the density is high enough, the fitted value of Γ becomes negative. In the absence of a quantitative prediction for Γ , we have not been able to give a meaning to such non-physical prediction—it could be a γ -dependent finite-size effect, a numerical instability caused by a value of Γ which is too small, or even a hint that the functional form of the decay is not exponential. Indeed, we find that for large γ , when the momentum of the special modes $q^*(\gamma/(2J))$ becomes comparable to the Fermi momentum k_F the decay is most likely a stretched exponential, albeit the analysis is obscured by the presence of oscillations.

Notwithstanding these caveats, it is relevant to understand the relation of Γ to the measurement rate, γ . Noticing the exponential decrease of Γ with the density, we assume $\ln \Gamma = a(\gamma) - f(\gamma)\bar{n}$ and we extract the coefficients with a linear fit against the density. The term $a(\gamma)$ is found to be an approximately linear function, whereas $f(\gamma)$ has a more interesting behavior that is shown in Fig. 2c. We find that $f(\gamma)$ grows at small γ , suggesting that the extra exponential decay may have a nonperturbative origin. Indeed, the double logarithmic plot of Fig. 2c shows a plausible power-law behavior, which we extract through a linear fit of the first 10 points as $f(\gamma) \approx 0.453/\gamma^{1.38}$. An accurate determination of Γ at small γ requires further work.

BOSONIZATION

In this Section we bosonize the non-Hermitian Hamiltonian $K = H - i\gamma/2n_0$ along the lines of [15] and [21]. We assume that the measured site is at $j_0 = 0$, and that the number of sites L is odd¹, and we define the symmetric c_{ks} and antisymmetric c_{ka} fermion operators according to

$$c_{\pm k} = \begin{cases} \frac{1}{\sqrt{2}}(c_{ks} \pm c_{ka}) , & \text{if } k > 0 , \\ c_{0s} , & \text{if } k = 0 , \end{cases} \quad (14)$$

which correspond to decomposing the real-space operators in operators which are symmetric or antisymmetric with respect to the origin:

$$c_j = \frac{1}{\sqrt{L}} \sum_k e^{ikj} c_k = \frac{1}{\sqrt{L}} c_{0s} + \sum_{k>0} \sqrt{\frac{2}{L}} \cos(kj) c_{ks} + \sum_{k>0} i \sqrt{\frac{2}{L}} \sin(kj) c_{ka} \equiv c_{js} + c_{ja} . \quad (15)$$

Correspondingly, as long as the band dispersion is even in momentum, $\varepsilon_{-k} = \varepsilon_k$, the free Hamiltonian separates into two symmetry sectors $H = H_s + H_a \equiv \sum_{k>0} \varepsilon_k c_{ks}^\dagger c_{ks} + \sum_{k>0} \varepsilon_k c_{ka}^\dagger c_{ka}$, and the ground state factorizes into two Fermi seas $|FS\rangle = |FS\rangle_s |FS\rangle_a$, both filled from momentum $k = 0$ to the Fermi momentum $k = k_F$. The imaginary potential scattering is proportional to $n_0 = c_{j=0,s}^\dagger c_{j=0,s}$, which involves the symmetric states only, hence the asymmetric states do not participate in the dynamics. As usual in bosonization, we need to adopt a continuum description in terms of a fermion field $\psi(x = ja) \equiv a^{-1/2} c_j$, with vanishing lattice spacing $a \rightarrow 0$. This field can be decomposed as above, $\psi(x) = \psi_s(x) + \psi_a(x)$. Then, we assume that all the dynamics occurs in the vicinity of the *single* Fermi point of the symmetric modes, so that we can restrict the degrees of freedom to those around $k = k_F$

$$\psi_s(x) = \frac{1}{\sqrt{L}} c_{0s} + \sum_{k>0} \frac{e^{ikx} + e^{-ikx}}{\sqrt{2L}} c_{ks} \approx \frac{1}{\sqrt{2}} [e^{ik_F x} R(x) + e^{-ik_F x} L(x)] , \quad (16)$$

where the right-movers $R(x)$ and left-movers $L(x)$ are

$$R(x) = \sum_{k: |k-k_F| < \alpha^{-1}} \frac{e^{i(k-k_F)x}}{\sqrt{L}} c_{ks} , \quad (17a)$$

$$L(x) = \sum_{k: |k-k_F| < \alpha^{-1}} \frac{e^{-i(k-k_F)x}}{\sqrt{L}} c_{ks} . \quad (17b)$$

with a suitable cutoff α . The left-movers are not independent of the right-movers: $L(x) = R(-x)$, so that there is actually only one chiral species of fermions. This happens because the symmetric sector has only one Fermi point. Notice also that the symmetrized fields have to be considered for $x > 0$ (or, equivalently, $x < 0$) only, to avoid doubling the degrees of freedom. Then, we can use $R(-x) = L(x)$ to define $R(x)$ on the whole axis. Finally, we linearize the dispersion around the Fermi point and express it in terms of $R(x)$ alone:

$$H_s - E_{\text{gs}} \approx \sum_{|k-k_F| < 1/\alpha} v_F(k - k_F) c_{ks}^\dagger c_{ks} = \int_{-La/2}^{La/2} dx R^\dagger(x) (-iv_F \partial) R(x) , \quad (18)$$

where $v_F \equiv \partial_k \varepsilon_k \big|_{k=k_F}$ is the Fermi velocity, equal to $2J \sin(\pi \bar{n})$ for lattice fermions. The one above is the standard Hamiltonian for chiral fermions, which can be bosonized in terms of a single bosonic field $\chi(x)$ with the usual formulae [14]:

$$R(x) = \frac{1}{\sqrt{2\pi\alpha}} F e^{-i\chi(x)} , \quad (19a)$$

$$\chi(x) = \phi(x) - \theta(x) = \frac{2i\pi}{\sqrt{L}} \sum_{q>0} \frac{V_q}{q} (b_q e^{iqx} - b_q^\dagger e^{-iqx}) . \quad (19b)$$

¹ For an even number of sites one needs to add another symmetric mode, $c_{\pi s} = c_\pi$ (assuming a Brillouin zone $p \in]-\pi, \pi[$). The presence of this mode does not affect the continuum results.

In the above, F is the Klein operator, while ϕ and θ are the usual TLL fields in the notation of [14].

The description of the system in terms of a single chiral field has an important technical consequence: the local imaginary potential is proportional to $\psi^\dagger(0)\psi(0) = \psi_s^\dagger(0)\psi_s(0) = 2R^\dagger(0)R(0)$, which does not contain any backscattering terms like $R^\dagger(0)L(0) + L^\dagger(0)R(0)$, which would give rise to nonlinear terms $\propto \cos(2\chi(0))$. Thus, using the standard relation [14, 15] $R^\dagger(x)R(x) = \frac{1}{2}\bar{\rho} - \frac{1}{2\pi}\partial\chi(x)$ [with $\bar{\rho} \equiv N_f/(La)$ the density of fermions], we find that the bosonized non-Hermitian Hamiltonian (for the symmetric modes) is quadratic in $\chi(x)$:

$$K_{TLL} = \frac{v_F}{2\pi} \int dx [\partial\chi(x)]^2 - i\gamma_c \left[\frac{1}{2}\bar{\rho} - \frac{1}{2\pi}\partial\chi(0) \right] = \sum_{q>0} \left[\varepsilon_q b_q^\dagger b_q - i \frac{\gamma_c}{\sqrt{L}} V_q (b_q + b_q^\dagger) \right] - i\gamma_c \frac{1}{2}\bar{\rho}, \quad (20)$$

where $\gamma_c = \gamma a$, $\varepsilon_q \equiv v_F q$ and $V_q \equiv q^{1/2} e^{-\alpha q}/(2\pi)$. We are dropping the finite-size contributions containing the Klein factors and we put the TLL subscript to emphasize that this Hamiltonian describes the system within the usual framework of Tomonaga-Luttinger liquids (TLLs). Indeed, we could generate nonlinear terms in K_{TLL} by considering the curvature of the dispersion relation [22], but this would bring us beyond the scope of TLLs.

To sum up, we have obtained a quadratic non-Hermitian Hamiltonian, and therefore we can obtain the full dynamics of the system. Using the Magnus expansion and the Baker-Campbell-Hausdorff formula [23], we can write

$$\begin{aligned} e^{-iK_{TLL}t} &= e^{i\text{Im} F(t) - \gamma_c \frac{1}{2}\bar{\rho}t} e^{-iH_{TLL}t} e^{\sum_q (\alpha_q^*(t) b_q^\dagger + \alpha_q(t) b_q)} = \\ &= e^{F(t) - \gamma_c \frac{1}{2}\bar{\rho}t} e^{-iH_{TLL}t} e^{\sum_q \alpha_q^*(t) b_q^\dagger} e^{\sum_q \alpha_q(t) b_q}, \end{aligned} \quad (21)$$

where $H_{TLL} \equiv \sum_{q>0} \varepsilon_q b_q^\dagger b_q$ and we introduced

$$F(t) \equiv \frac{\gamma_c^2}{L} \sum_{q>0} V_q^2 \frac{1 - i\varepsilon_q t - e^{-i\varepsilon_q t}}{\varepsilon_q^2} = \frac{\gamma_c^2}{(2\pi v_F)^2} \left(\ln \frac{\alpha + i v_F t}{\alpha} - i \frac{v_F t}{\alpha} \right) \quad (22)$$

(where the second equality refers to the continuum limit) and

$$\alpha_q(t) \equiv i \frac{\gamma_c}{\sqrt{L}} V_q \frac{1 - e^{-i\varepsilon_q t}}{\varepsilon_q}. \quad (23)$$

In the bosonic language, the initial state $|FS\rangle_s$ is simply the boson vacuum $|\omega\rangle$, hence the unnormalized state is

$$|\tilde{\psi}(t)\rangle \equiv e^{-iK_{TLL}t} |\omega\rangle = e^{2\text{Re} F(t) - \gamma_c \frac{1}{2}\bar{\rho}t} e^{i\text{Im} F(t)} |\text{coh}[\alpha_q^*(t) e^{-i\varepsilon_q t}]\rangle, \quad (24)$$

where $|\text{coh}[z_q]\rangle \equiv e^{\sum_q (z_q b_q^\dagger - z_q^* b_q)} |\omega\rangle$ is a bosonic coherent state, and we used

$$\begin{aligned} e^{\sum_q \alpha_q^* b_q^\dagger} |\omega\rangle &= e^{\frac{1}{2} \sum_q |\alpha_q|^2} |\text{coh}[\alpha_q^*]\rangle, \\ e^{-i \sum_q \theta_q b_q^\dagger b_q} |\text{coh}[z_q]\rangle &= |\text{coh}[z_q e^{-i\theta_q}]\rangle \end{aligned}$$

and $\frac{1}{2} \sum_q |\alpha_q(t)|^2 = \text{Re} F(t)$. Finally, we obtain the normalized state

$$|\psi(t)\rangle = \frac{|\tilde{\psi}(t)\rangle}{\langle \tilde{\psi}(t) | \tilde{\psi}(t) \rangle^{1/2}} = e^{i\text{Im} F(t)} |\text{coh}[\alpha_q^*(t) e^{-i\varepsilon_q t}]\rangle. \quad (25)$$

We notice that this result is almost identical to the one that we would obtain in the Hermitian case (i.e. for $\gamma \rightarrow -iV$).

It is easy to compute the return amplitude using the property of the coherent states that $\langle \omega | \text{coh}[z_q] \rangle = e^{-\frac{1}{2} \sum_q |z_q|^2}$:

$$\mathcal{L}(t) = \langle \omega | \psi(t) \rangle = e^{-F(t)}, \quad (26)$$

and from Eq. (22) we can read off that for times $v_F t \gg \alpha$ we have $|\mathcal{L}(t)| \sim [\alpha/(v_F t)]^{\beta_b}$, where

$$\beta_b = \frac{\gamma_c^2}{(2\pi v_F)^2} \quad (27)$$

is the bosonization prediction quoted in the main text. The above result is the same as in the Hermitian case of a scattering potential with strength $\gamma_c/2$.

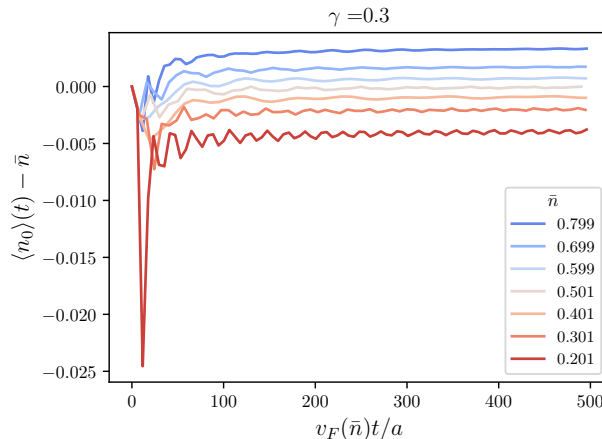


FIG. 3. Time evolution of the fermion density at the impurity site.

The energy injected by the measurement can be computed as follows:

$$\begin{aligned}
 E(t) &= \langle \psi(t) | H_{TLL} | \psi(t) \rangle = \sum_{q>0} \varepsilon_q |\alpha_q(t)|^2 = \frac{\gamma_c^2}{L} \sum_{q>0} \varepsilon_q V_q^2 2 \frac{1 - \cos(\varepsilon_q t)}{\varepsilon_q^2} = \\
 &= 2 \frac{\gamma_c^2}{(2\pi)^2 v_F} \int_0^{+\infty} dq e^{-\alpha q} [1 - \cos(qv_F t)] = \frac{\gamma_c^2}{2\pi^2 v_F} \left[\frac{1}{\alpha} - \text{Re} \frac{1}{\alpha + iv_F t} \right] \xrightarrow{t \rightarrow +\infty} \frac{\gamma_c^2}{2\pi^2 v_F \alpha}.
 \end{aligned} \tag{28}$$

Although the exact value of the energy is cutoff-dependent (as expected for an effective low-energy description such as the TLL), it is predicted to saturate.

The time-dependence of the density at the measured site can be computed similarly:

$$\begin{aligned}
 \langle \psi^\dagger(0) \psi(0) \rangle_t - \bar{\rho} &= 2 \langle R^\dagger(0) R(0) \rangle_t - \bar{\rho} = -\frac{1}{\pi} \langle \partial \chi(0) \rangle_t = \frac{2}{L^{1/2}} \sum_{q>0} V_q \langle b_q + b_q^\dagger \rangle_t = \\
 &= \text{Im} \frac{4\gamma_c}{L} \sum_{q>0} V_q^2 \frac{1 - e^{-i\varepsilon_q t}}{\varepsilon_q} = \text{Im} \frac{\gamma_c}{\pi^2 v_F} \int_0^{+\infty} dq e^{-\alpha q} (1 - e^{-iqv_F t}) = -\frac{\gamma_c}{\pi^2 v_F} \frac{v_F t}{\alpha^2 + (v_F t)^2}.
 \end{aligned} \tag{29}$$

Thus, the prediction of the bosonized model is that the density at the measured site should decrease almost linearly up to a cutoff-dependent time α/v_F , after which it would start increasing again until returning asymptotically to the initial value. This is not what the numerics shows. In Fig. 3 we report the typical time evolution of the density at the measured site $\langle n_0 \rangle(t)$ for different initial densities. Also in this observable, we find a monotonic behavior as a function of the density, with $\langle n_0 \rangle(t)$ saturating to a value which grows with \bar{n} , and that is smaller (larger) than \bar{n} approximately below (above) half-filling. So, the bosonization prediction (29), in which $\langle n_0 \rangle(t)$ should return back to the original value after a transient, is valid only in the vicinity of half-filling (including the sharp decrease at small times, which is however not universal). We notice that the interpretation of the dynamics of the system in real space is not intuitive, as the time evolution induced by non-Hermitian Hamiltonians is nonlocal due to the lack of a Lieb-Robinson bound [24].

We can have an intuition about why the bosonized model does not agree with the numerical results by noticing that it has a larger symmetry than the discrete one. Indeed, if we drop the constant shift $-i\gamma_c \bar{\rho}/2$, the non-hermitian hamiltonian K_{TLL} is \mathcal{PT} symmetric [24], where \mathcal{T} is the anti-unitary time-reversal operator, while the parity operator \mathcal{P} changes the sign of $\chi(x)$. As long as the symmetry is unbroken, it implies that the eigenvalues of K_{TLL} are all in the form $\mathcal{E} - i\gamma_c \bar{\rho}/2$, where \mathcal{E} is real. In other words, all eigenstates of the K_{TLL} decay with the same lifetime, $\gamma_c \bar{\rho}/2$. On the other hand, as we will show in the next section, the discrete non-Hermitian Hamiltonian does not have such a symmetry, since the imaginary part of its spectrum is not constant². The existence of a variety of lifetimes

² An unbroken \mathcal{PT} symmetry is a sufficient condition [24] for a *real* spectrum, but here we are extending the notion to within an *imaginary* shift of the Hamiltonian. Such a constant shift is unobservable in the nonlinear Schrödinger equation, just as a real energy shift does not have any observable consequences for Hermitian Hamiltonians.

implies that the nonlinear Schrödinger equation (1) will bring the state to converge to the many-body eigenstate of K that has the lowest imaginary part (or the highest, for $\gamma < 0$). This convergence will happen on a timescale that is extensive in the system size (we have numerically verified that it is usually much larger than L/v_F), so that the dynamics that we are interested in occurs in a time regime (i.e. for times smaller than $L/(2v_F)$) in which the system state is still very far from the stationary one. Nonetheless, this equilibration dynamics is completely absent in the bosonized model, since a constant imaginary part of the eigenvalues of K cancels out of the dynamics in Eq. (1). As a consequence, we expect K_{TLL} to behave effectively as a Hermitian Hamiltonian, and this is what we observed in the explicit solution outlined above, which is analogous to the one in the usual OC. As a final remark, we will show that the discrete version of K does have an approximate \mathcal{PT} symmetry, since it features a large number of eigenvalues that have essentially the same imaginary part. We believe that this is the reason why the bosonized mode is able to correctly predict the OC behavior (i.e. the algebraic decay of $\mathcal{L}(t)$) that we observe.

SPECTRAL PROPERTIES OF NON-HERMITIAN HAMILTONIAN

The non-Hermitian Hamiltonian K has been already considered in [25] and [8], but from points of view that differ from the present work. The first one considered the single-particle scattering properties of K , but employed open boundary conditions. The second one focused on the “strong-coupling” regime $\gamma \geq 4J$ and on the continuum limit, which is not relevant for the results presented in this work, since we are especially interested in the scattering properties in the “weak-coupling” regime $\gamma < 4J$, which require to consider a finite-size system. Thus, although many of the results of this section are known, it is useful to gather them together for completeness.

Analytic relations

It is convenient to work in momentum space, in which $K = \sum_{p,q} c_p^\dagger \kappa_{pq} c_q$, where the single-particle Hamiltonian κ reads $\kappa_{pq} = \varepsilon_q \delta_{pq} - \frac{i\gamma}{2L}$. The single-particle right eigenfunctions $\langle k|r_\alpha \rangle$ satisfy $\sum_k \kappa_{pk} \langle k|r_\alpha \rangle = \lambda_\alpha \langle p|r_\alpha \rangle$, or

$$\varepsilon_p \langle p|r_\alpha \rangle - i \frac{\gamma}{2L} \sum_k \langle k|r_\alpha \rangle = \lambda_\alpha \langle p|r_\alpha \rangle ,$$

from which we extract

$$\langle p|r_\alpha \rangle = i \frac{\gamma}{2L} \frac{S_\alpha}{\varepsilon_p - \lambda_\alpha} , \quad (30)$$

where $S_\alpha \equiv \sum_k \langle k|r_\alpha \rangle$. Introducing the real-space eigenfunctions $\langle j|r_\alpha \rangle = L^{-1/2} \sum_p e^{ipj} \langle p|r_\alpha \rangle$ we recognize that³ $S_\alpha = \sqrt{L} \langle j=0|r_\alpha \rangle$. Self-consistency requires either $S_\alpha = 0$ or

$$1 = i \frac{\gamma}{2L} \sum_p \frac{1}{\varepsilon_p - \lambda_\alpha} , \quad (31)$$

which determines the nontrivial eigenvalues. The solutions with $S_\alpha = 0$ are just the antisymmetric modes, which are unaffected by the impurity. Taking the conjugate of Eq. (31) we find that $\lambda_\alpha(-\gamma) = \lambda_\alpha(\gamma)^*$.

The left eigenstates satisfy $\sum_k \langle l_\alpha|k \rangle \kappa_{kp} = \lambda_\alpha \langle l_\alpha|p \rangle$, but since $\kappa = \kappa^T$ is symmetric, $\langle l_\alpha|k \rangle$ is determined by the same equation as $\langle p|r_\alpha \rangle$, so $\langle l_\alpha|p \rangle = \langle p|r_\alpha \rangle$. The S_α are fixed by normalizing the states according to $\langle l_\alpha|r_\beta \rangle = \delta_{\alpha\beta}$:

$$\langle l_\alpha|r_\beta \rangle = \left(\frac{i\gamma}{2L} \right)^2 S_\alpha S_\beta \sum_p \frac{1}{\varepsilon_p - \lambda_\alpha} \frac{1}{\varepsilon_p - \lambda_\beta} .$$

For $\lambda_\alpha \neq \lambda_\beta$ the sum is

$$i \frac{\gamma}{2L} \sum_p \frac{1}{\varepsilon_p - \lambda_\alpha} \frac{1}{\varepsilon_p - \lambda_\beta} = \frac{1}{\lambda_\alpha - \lambda_\beta} i \frac{\gamma}{2L} \sum_p \left[\frac{1}{\varepsilon_p - \lambda_\alpha} - \frac{1}{\varepsilon_p - \lambda_\beta} \right] = 0 ,$$

³ In this section, we set $j_0 = 0$.

where the last equality comes from Eq. (31). Numerically, the spectrum is nondegenerate, so

$$S_\alpha^{-1} = i \frac{\gamma}{2L} \left[\sum_p \frac{1}{(\varepsilon_p - \lambda_\alpha)^2} \right]^{1/2}. \quad (32)$$

An important quantity is the overlap $\langle r_\alpha | r_\beta \rangle$:

$$\langle r_\alpha | r_\beta \rangle = \left(\frac{\gamma}{2L} \right)^2 \sum_p \frac{1}{\varepsilon_p - \lambda_\alpha^*} \frac{1}{\varepsilon_p - \lambda_\beta}.$$

The sum can be computed as above:

$$i \frac{\gamma}{2L} \sum_p \frac{1}{\varepsilon_p - \lambda_\alpha^*} \frac{1}{\varepsilon_p - \lambda_\beta} = \frac{1}{\lambda_\alpha^* - \lambda_\beta} i \frac{\gamma}{2L} \sum_p \left[\frac{1}{\varepsilon_p - \lambda_\alpha^*} - \frac{1}{\varepsilon_p - \lambda_\beta} \right] = -\frac{2}{\lambda_\alpha^* - \lambda_\beta},$$

and so we obtain

$$\langle r_\alpha | r_\beta \rangle = i \frac{\gamma}{L} \frac{S_\alpha^* S_\beta}{\lambda_\alpha^* - \lambda_\beta}. \quad (33)$$

As $\text{sgn}(\text{Im } \lambda_\alpha) = -\text{sgn}(\gamma)$, $\lambda_\alpha^* \neq \lambda_\beta$ is always valid.

The normalization constants satisfy $\sum_\alpha S_\alpha^2 = L$, since

$$\sum_\alpha S_\alpha^2 = \sum_\alpha \sum_{p,k} \langle p | r_\alpha \rangle \langle k | r_\alpha \rangle = \sum_\alpha \sum_{p,k} \langle p | r_\alpha \rangle \langle l_\alpha | k \rangle = \sum_{p,k} \langle p | \sum_\alpha | r_\alpha \rangle \langle l_\alpha | | k \rangle = \sum_{p,k} \langle p | k \rangle = L,$$

where we used the completeness relation [24] $\sum_\alpha | r_\alpha \rangle \langle l_\alpha | = \mathbb{1}$. Another useful relation can be found by taking the derivative of Eq. (31) with respect to γ : we find that

$$\frac{\partial \lambda_\alpha}{\partial \gamma} = -\frac{i}{2L} S_\alpha^2 (\{\lambda_\beta(\gamma)\}, \gamma) = -\frac{i}{2} \langle j=0 | r_\alpha \rangle^2, \quad (34)$$

which connects the spectrum with the value of the right eigenfunctions at the measured site.

Spectrum of non-Hermitian Hamiltonian

Equation (31) needs to be solved numerically to determine the eigenvalues, or, equivalently, one can diagonalize κ_{pq} numerically. Most of the qualitative results are largely known from [8, 25], and we repeat them in some detail. In the ‘‘weak-coupling’’ regime $\gamma \leq 4J$, the eigenstates are similar to the scattering states in the Hermitian case [26]: the eigenvalues λ_α occur close to the original eigenvalues ε_p , hence we can label them with the corresponding momentum:

$$\lambda_p = \varepsilon_p - v_p \frac{2\pi}{L} \frac{\delta_p}{\pi}, \quad (35)$$

where $v_p \equiv \partial_p \varepsilon_p = 2J \sin p$ is the local group velocity, and as customary we have parametrized the correction to the energies in terms of a scattering phase δ_p , which in this non-Hermitian case is *complex*. As discussed in the previous Section, only the symmetric modes interact with the impurity, so the momenta p belong to the halved Brillouin zone $p \in [0, \pi]$ (in which $v_p \geq 0$).

We notice that the correction $\lambda_p - \varepsilon_p$ is of order L^{-1} , implying that in the $\gamma \leq 4J$ regime one cannot directly take the continuum limit $L^{-1} \sum_p \rightarrow (2\pi)^{-1} \int dp$ in Eq. (31), since λ_p depends on L as well [and hence the sum in Eq. (31) is not a Riemann sum]. The approximate method described in [26] may be used, instead. Another point that may need some clarification is the large size limit $L \rightarrow +\infty$. If we take this limit with Eq. (35) we obtain $\lambda_p \rightarrow \varepsilon_p$, which seems to imply that in the large size limit we would recover the physics of noninteracting fermions. This actually implies only that the large size limit is not suitable for a single particle. But we are interested in a many-particle system in the thermodynamic limit, in which not only the system size grows but also the number of particles N_f does, such that the density $\bar{n} = N_f/L$ remains constant. In this limit, the *many-body* eigenvalues of K are well-defined, since they are sums over the occupied states $\mathbf{p} = (p_1, \dots, p_{N_f})$, $\Lambda_{\mathbf{p}} = \sum_{j=1}^{N_f} \lambda_{p_j}$, for which the

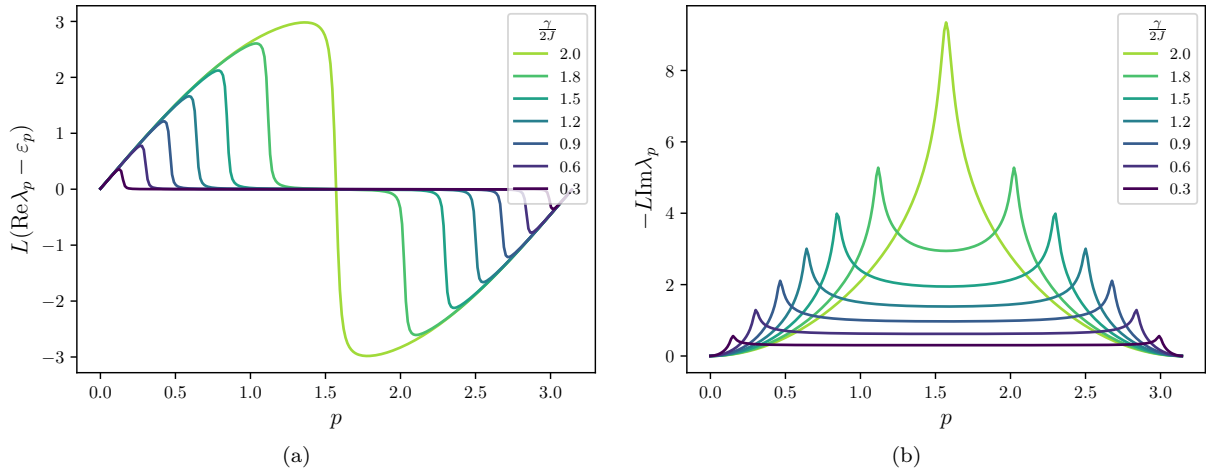


FIG. 4. Single-particle spectrum of K up to the exceptional point, $\gamma \leq 4J$. (a) Real part (b) Imaginary part. Notice that the values have been multiplied by the system size L .

correction is $\Lambda_{\mathbf{p}} - \sum_{j=1}^{N_f} \varepsilon_{p_j} = 2\overline{v\delta} N_f/L = 2\overline{v\delta} \bar{n}$ ($\overline{v\delta}$ is the arithmetic average of $v_p\delta_p$ over the occupied states), which is finite in the thermodynamic limit.

Figure 4 shows the spectrum of κ for a system of $L = 500$ sites for various values of $\gamma \leq 4J$. The left panel displays the real part of $\lambda_p - \varepsilon_p$ (proportional to the real part of δ). We observe that, except for γ close to $4J$, there are corrections mainly at the edges of the band (i.e. for p close to 0 or π).

The right panel of Fig. 4 shows the imaginary part of λ_p (which is completely contained in δ_p), and displays most of the physics that we are interested in. For all $\gamma < 4J$, $-\text{Im} \lambda_p$ has a common structure: it is almost vanishing at the very edges of the band, then it has a peak up to about $2\gamma/L$ at some special momenta q^* and $\pi - q^*$, until it settles to an almost constant value close to⁴ γ/L for all momenta in a region in the middle of the band. Thus, we see that the description provided by bosonization is accurate for the states not too far from mid-band, which have roughly the same imaginary part of λ_p and are expected to behave similarly to a Hermitian system, as discussed at the end of the previous Section. We can also say that there is an emergent \mathcal{PT} symmetry. But this symmetry is explicitly broken close to the band edges, where $\text{Im} \lambda_p$ varies abruptly. In all the numerical results that we presented in the main text, the Fermi surface lies far from the band edges. Therefore, the linearization of the spectrum close to $p = k_F$ cannot possibly account for these special modes, and we understand what is being missed by bosonization. Curiously, the feature that brings about the failure of bosonization is not in the real part of the spectrum, that is, the band dispersion, but rather in the imaginary part, hence the lifetime of the states.

To show that this intuition is correct, and that the enhanced decay rate at the special momenta q^* does affect the dynamics, we report in Fig. 5 the momentum occupancy $n_q \equiv \langle c_q^\dagger c_q \rangle$ in the full Brillouin zone for $L = 1000$ sites at a given time and at a fixed value of $\gamma/(2J)$, while the density is varied from one curve to the other. This occupancy can be computed from the Fourier transform of the real-space correlation function $\langle c_i^\dagger c_j \rangle$, which is easily computed with the algorithm of [20]. From the Fig., we see that the Fermi surface is still well-defined, and only rounded by the potential scattering. This is exactly the kind of process that is described by bosonization. On the other hand, there is an extra depletion of population at two momenta close to $q = 0$, and it turns out that these momenta are exactly corresponding to the special momenta $\pm q^*$ ($p = q^*$ in the half-Brillouin zone of the symmetric modes corresponds to $p = \pm q^*$ in the whole Brillouin zone). Unless the density is sufficiently high, the special states at the top of the band, $p = \pm(\pi - q^*)$ are not populated enough to show any nontrivial dynamics. The important observation on Fig. 5 is that the rate of depletion of the special modes is larger at smaller densities. This property can be taken as a clue that the special modes play a more relevant role at lower densities. Such conclusion fits precisely into our intuition that the special modes are the ones responsible for the breakdown of bosonization and it is agreement with the numerical results showing that the return amplitude and the energy absorption depart from bosonization more strongly at lower densities. Actually, the momentum occupation is directly related to the absorbed energy, $E(t) = \sum_q \varepsilon_q n_q(t)$, and it is easy to see that $E(t)$ has to rise faster than what bosonization predicts, since the states removed from around

⁴ This value can be easily computed from first order degenerate perturbation theory.

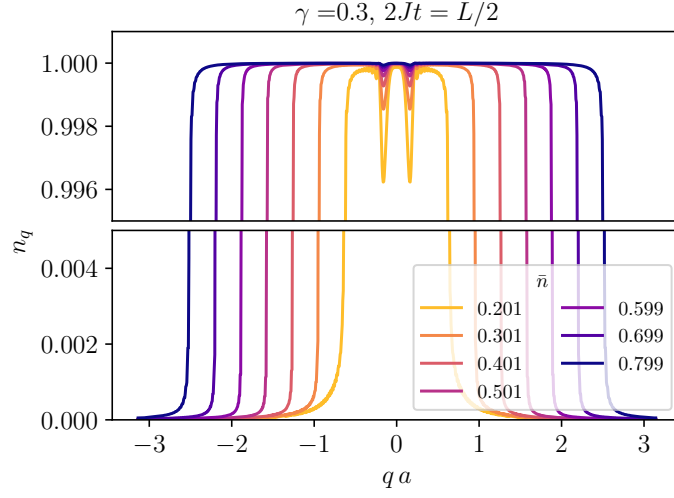


FIG. 5. Momentum occupancy $n_q(t) = \langle \psi(t) | c_q^\dagger c_q | \psi(t) \rangle$ at a fixed time, showing the extra depletion at the special momenta deep within the Fermi sea.

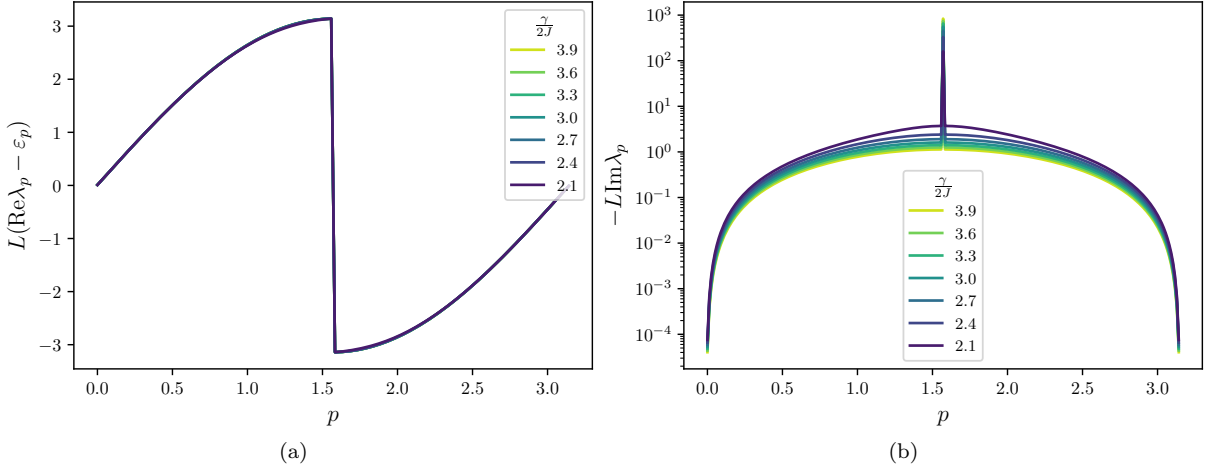


FIG. 6. Single-particle spectrum of K above the critical point, $\gamma > 4J$. (a) Real part, which is almost insensitive to the value of γ (b) Imaginary part, showing the large peak at the bound state (notice the logarithmic scale).

$|q| = q^*$, which have low energy, must be moved to unoccupied states at high energy $\varepsilon_p > \varepsilon_F$ because of particle number conservation and the exclusion principle. On the other hand, there is no direct relation between n_q and the return amplitude $\mathcal{L}(t)$.

We have not been able to derive a quantitative relation between the density and the effect of the special modes. Indeed, the momentum of the depletions in $n_q(t)$ decreases in time towards $\pm q^*$, and the value of q^* itself does not depend on \bar{n} since it is a property of the single-particle states. The numerics and the approximate formula for λ_p that we derive later suggest that q^* is (at least approximately) determined by the condition that the group velocity v_p of the fermions is equal to the strength of the potential $\gamma/2^5$, i.e.

$$q^* \approx \arcsin \frac{\gamma}{4J} . \quad (36)$$

This relation has already emerged in Ref. [25], as the momentum at which the imaginary potential scatters the incoming single-particle wave packets most effectively.

⁵ From Eq. (35) and the observation $-\text{Im} \lambda_{q^*} \approx 2\gamma/L$ we deduce that $\delta_{q^*} \approx 2i$.

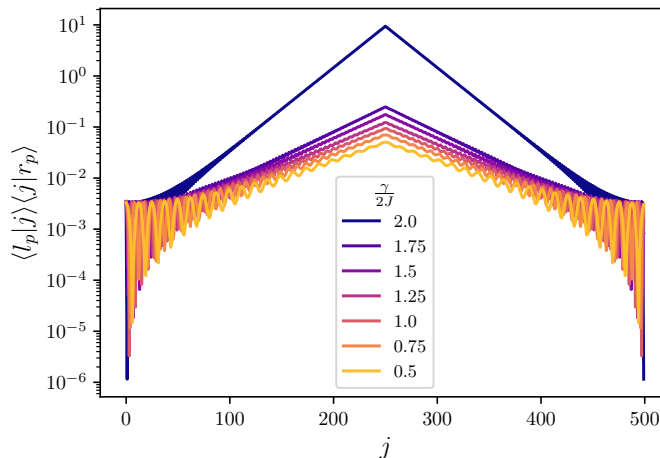


FIG. 7. Special modes in real space. We are plotting $\langle l_p | j \rangle \langle j | r_p \rangle = |\langle j | r_p \rangle|^2$ as a function of j for $p = q^* = \arcsin(\gamma/(4J))$. We have taken $L = 500$ sites, with the impurity sitting at $j_0 = L/2$. We observe an exponentially decaying profile close to j_0 , reminiscent of a bound state, although the decay length is comparable to L . A true bound state emerges only at the exceptional point, $\gamma = 4J$, shown here as the upper blue curve.

Of course, the above equation suggests that something else must be happening when $\gamma \geq 4J$. Although this “strong-coupling” regime is beyond the numerical work presented in the main text, we report what it happens for completeness. Most of the properties of this regime have been already analyzed in [8], in the limit $L \rightarrow +\infty$. From Fig. 4 and Eq. (36) we observe that for $\gamma = 4J$ the two peaks merge into one. This value of γ marks an exceptional point [24], namely a point in the parameter space of K in which the non-Hermitian Hamiltonian is not diagonalizable because the two special eigenstates coalesce to the same vector. For γ above the critical value $4J$ the matrix becomes diagonalizable again and the spectrum reorganizes completely, as shown in Fig. 6: almost all of the imaginary part (right panel in Fig. 6) becomes concentrated⁶ on a single state in the middle of the band $p = \pi/2$, which acquires a decay rate of the order of $\gamma/2$, whereas the rest of the eigenvalues have a rather small imaginary part (notice the logarithmic scale of the Figure). The corrections to the real part of the eigenstates (left panel in Fig. 6) remain small and scarcely dependent on γ . The analytic dependence on γ of the imaginary part of the special eigenvalue can be found in [6, 8], since it is the only one that survives also in the large size limit $L \rightarrow +\infty$, so that it can be obtained by transforming the sum in Eq. (31) in an integral over momenta and solving for λ .

The above discussion provides a reasonably clear picture of why bosonization fails in our model of non-Hermitian OC, but it leaves the physical nature of the special modes somewhat unspecified. A better understanding comes from considering their wavefunctions⁷ in real space, as shown in Fig. 7. Close to $j = j_0 = L/2$ we can observe the typical exponential envelope of a bound state, except that the tails of the wavefunction far from the measured site decay much slower. We can say that the special modes are quasi-bound states, whose size is comparable to the length of the system but which are pinned at the impurity site, experiencing a stronger potential and hence an enhanced decay rate. At the exceptional point the two states merge and a true bound state is created [8].

We can give an approximate expression for the scattering phase δ_p , using the relation (34). Following [26], we can approximate S_p as

$$S_p \approx -i \frac{\sqrt{8}v_p}{\gamma} \sin \delta_p, \quad (37)$$

which is quite close to the numerical data. Substituting the equation in Eq. (34) and solving the resulting differential equation we obtain

$$\cot \delta_p(\gamma) + \frac{2iv_p}{\gamma} \approx \theta_p, \quad (38)$$

⁶ The sum of all imaginary parts is fixed by the trace of K : $\sum_p \text{Im } \lambda_p = \text{Im Tr } K = -\gamma/2$.

⁷ Since κ is symmetric, we can consider equally the right or the left eigenstates.

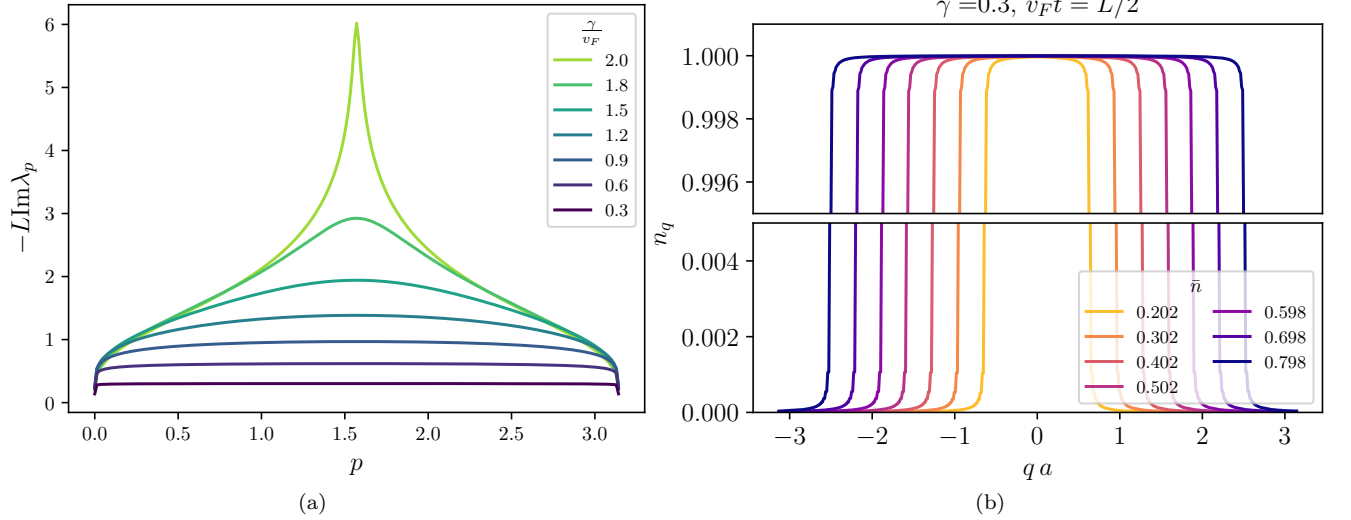


FIG. 8. Properties of the non-Hermitian Tomonaga Hamiltonian in momentum space. (a) Imaginary part of the spectrum of K for $L = 500$ and $v_F = 1$, below the exceptional point $\gamma \leq 2v_F$. The imaginary part is essentially flat, except near the $\gamma = 2v_F$. (b) Momentum occupancy at a fixed time for $L = 500$, $v_F = 1$, showing the absence of dynamics deep in the Fermi sea.

in which θ_p is a function that does not depend on γ . Unfortunately, the limit $\gamma \rightarrow 0$, in which $\delta_p \rightarrow 0$, cannot be used to set the value of θ_p , because both $\cot \delta_p$ and $1/\gamma$ diverge. If we set $\theta_p = 0$ we obtain

$$\delta_p \approx \begin{cases} -\frac{\pi}{2} \operatorname{sgn}(\frac{\pi}{2} - p) + i \operatorname{arctanh} \frac{\gamma}{2v_p} & \text{for } \gamma < v_p, \\ i \operatorname{arctanh} \frac{2v_p}{\gamma} & \text{for } \gamma > v_p, \end{cases} \quad (39)$$

which is a rough approximation for $\operatorname{Re} \delta_p$ but a quite good one for $\operatorname{Im} \delta_p$ (except for v_p close to $\gamma/2$, i.e. the special modes). In particular, we find that $\delta_p \approx i \frac{\gamma}{2v_p}$ to lowest order in γ and in the middle of the band (i.e. for $\gamma < v_p$), which yields the result of bosonization: $\beta = \frac{|\delta_{k_F}^2|}{\pi^2} \approx \frac{\gamma^2}{(2\pi v_F)^2}$, using the exact relation between β and δ_p [26, 27].

The role of band curvature

There is another aspect that is important to mention: the condition (36) implies that the presence of the special, quasi-bound modes is due to the variation of the group velocity of the fermions—in other words, it is a consequence of the band curvature. To confirm this picture, we have repeated the various numerical calculations with an artificial model that features linearly-dispersing fermions, i.e. we have set $\varepsilon_q = v_F |q|$ for $|q| \leq \pi$ and periodically repeated for other momenta. This is known as Tomonaga model [13]. In Fig. 8a we show the imaginary part of the single-particle eigenvalues of K for $L = 500$ and increasing values of γ/v_F . The appearance of the spectrum is quite different from the previous case, with an imaginary part which is almost completely flat for small γ (except for very close to the band edges). The decay rates acquire some curvature only in the vicinity of the exceptional point $\gamma/2 = v_F$ [which is the same condition as Eq. (36)], at which point a bound state forms, analogously to the previous case. In agreement with the flatness of the single-particle decay rates, we observe no extra depletions in the momentum occupancies, as shown in Fig. 8b.

If our theory about the relation between a flat imaginary part of the spectrum and the validity of bosonization is valid, then we should observe that the various observables should be in agreement with the predictions from K_{TLL} . Indeed this prediction is confirmed, as shown in Figs. 9. In the upper panel, we show that the return amplitude $\mathcal{L}(t)$ is a pure power-law for various densities and values of γ , and that at late times it is in good agreement even with the finite-size prediction from bosonization $\mathcal{L}(t) = \exp(-F_L(t))$, with

$$F_L(t) \equiv \frac{\gamma_c^2}{L} \sum_{q>0} V_q^2 \frac{1 - i\varepsilon_q t - e^{-i\varepsilon_q t}}{\varepsilon_q^2} = \beta_b \ln \frac{1 - e^{-2\pi(\alpha + iv_F t)/L}}{1 - e^{-2\pi\alpha/L}}, \quad (40)$$

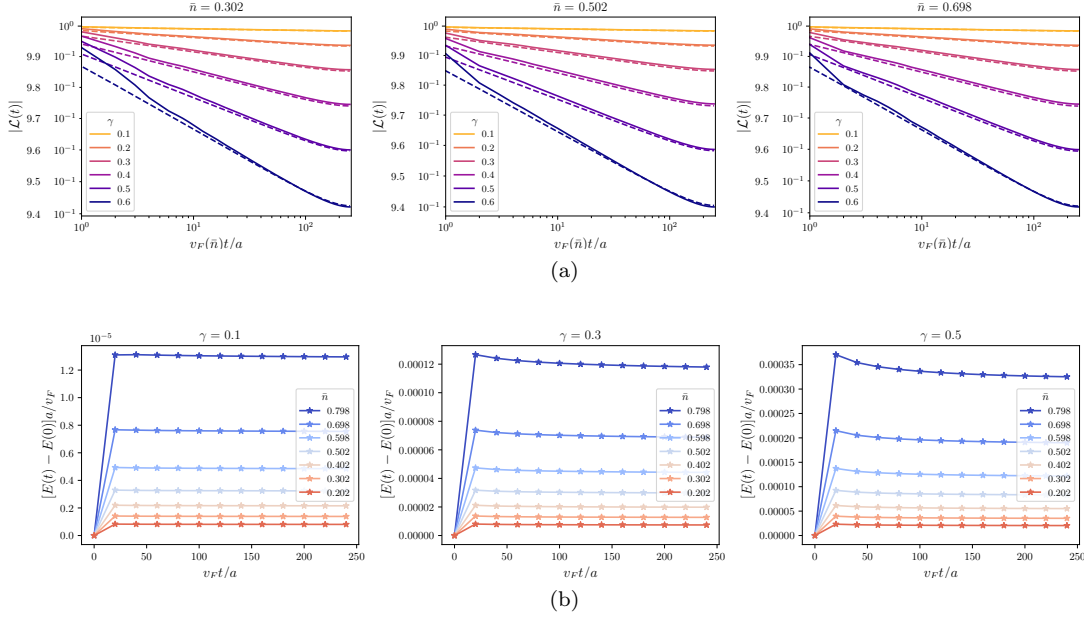


FIG. 9. Observables for the Tomonaga model with $L = 500$ and $v_F = 1$, showing agreement with bosonization. (a) The return amplitude (continuous lines) at various values of γ and \bar{n} compares with the prediction from finite-size bosonization (dashed lines). (b) The absorbed kinetic energy saturates, in agreement with bosonization.

whose only free parameter is the UV cutoff α . The lower panel shows that the kinetic energy absorbed by the system saturates, in agreement with the predictions from bosonization. Moreover, particle-hole symmetry (i.e. invariance of observables for reciprocal densities \bar{n} and $1 - \bar{n}$) is restored for the return amplitude. It is obvious that, since the imaginary part of the spectrum is not exactly flat (Fig. 8a), bosonization will eventually break down. However, for γ sufficiently far from the exceptional point, the timescale of the breakdown (i.e. what would be Γ , the rate of exponential decay of $\mathcal{L}(t)$) is pushed to very large values.

The conclusion from this discussion is that the effects that we observe beyond bosonization belong to the so-called beyond-Luttinger physics [22], in the sense that they are corrections to the predictions of bosonization that stem from the inability of the latter to take into account the curvature of the fermionic band dispersion. Similarly to the standard beyond-Luttinger phenomena, such as the presence of X-ray edges in the dynamical structure factor, these effects are non-perturbative in nature. On the other hand, rather than being consequences of the band curvature in the vicinity of the Fermi surface, the new phenomena depend on the curvature far from it—actually, from the very edge of the band.

CRUCIAL ROLE OF POST-SELECTION

In this section we show how post-selection is crucial for the result we presented in the main text. First, we are going to prove how the nonlinear dynamics dictated by post-selection is responsible for making the effects beyond bosonization more apparent. Then, we are going to present the opposite case of complete absence of post-selection, comparing our results with the case of localized dephasing.

Importance of nonlinear dynamics: cumulant expansion

The nonlinear dynamics induced by measurements seems to be crucial to expose the effects beyond bosonization. Indeed, the return amplitude is given by the ratio

$$\mathcal{L}(t) = \frac{\langle FS | \tilde{\psi}(t) \rangle}{\langle \tilde{\psi}(t) | \tilde{\psi}(t) \rangle^{1/2}}, \quad (41)$$

and it is easy to see that if we took only the numerator, $\tilde{\mathcal{L}}(t) = \langle FS|\tilde{\psi}(t)\rangle = \langle FS|e^{-iKt}|FS\rangle$ (the “unrenormalized” return amplitude) we would obtain a leading exponential decay $e^{-\gamma\bar{n}t/2}$. This can be seen by expanding in γ :

$$\begin{aligned}\tilde{\mathcal{L}}(t) &= e^{-iE_{FS}t} \langle FS|\mathcal{T}e^{-\gamma/2 \int_0^t dt' n_0(t')}|FS\rangle = \\ &= e^{-iE_{FS}t} \left[1 - \frac{\gamma}{2} \int_0^t dt' \langle n_0(t')\rangle + \left(\frac{\gamma}{2}\right)^2 \int_0^t dt_1 \int_0^{t_1} dt_2 \langle n_0(t_1)n_0(t_2)\rangle + \mathcal{O}(\gamma^3) \right] = \\ &= e^{-iE_{FS}t} \left[1 - \frac{\gamma}{2}\bar{n}t + \left(\frac{\gamma}{2}\right)^2 \int_0^t dt_1 \int_0^{t_1} dt_2 \langle n_0(t_1)n_0(t_2)\rangle + \mathcal{O}(\gamma^3) \right]\end{aligned}$$

where $E_{FS} = \langle FS|H|FS\rangle$, $\langle \cdot \rangle$ is the average on the ground state and $n_0(t) \equiv e^{iHt}n_0e^{-iHt}$ is the number operator at the measured site in the interaction picture. Then, we assume $\tilde{\mathcal{L}}(t) = \exp[-iE_{FS}t + \tilde{L}_1 + \tilde{L}_2 + \mathcal{O}(\gamma^3)] = \exp[-iE_{FS}t][1 + \tilde{L}_1 + \tilde{L}_2 + \mathcal{O}(\gamma^3)]$, where $\tilde{L}_k = \mathcal{O}(\gamma^k)$, and we determine $\tilde{L}_{1,2}$ by comparing with the direct expansion in γ , reported above: $\tilde{L}_1 = -\gamma\bar{n}t/2$, $\tilde{L}_2 = (\frac{\gamma}{2})^2 \int_0^t dt_1 \int_0^{t_1} dt_2 \langle (n_0(t_1) - \bar{n})(n_0(t_2) - \bar{n}) \rangle$. By expressing $n_0(t)$ in terms of momentum modes, the latter integral can be evaluated to

$$\tilde{L}_2 = \left(\frac{\gamma}{2}\right)^2 \frac{1}{L^2} \sum_{|p_1| < k_F} \sum_{k_F < |p_2| < \pi} \frac{1 + i(\varepsilon_{p_1} - \varepsilon_{p_2})t - e^{i(\varepsilon_{p_1} - \varepsilon_{p_2})t}}{(\varepsilon_{p_1} - \varepsilon_{p_2})^2},$$

where $k_F = \pi\bar{n}$ is the Fermi momentum. At long times, the sum is dominated by the terms with $\varepsilon_{p_1} \approx \varepsilon_{p_2}$ which due to the limits in the sums implies that both momenta have to be close to the Fermi surface. If we linearize the energy in this area, we find $\tilde{L}_2 \approx F(t) \sim -i\Delta\varepsilon t + \beta_b \ln(v_F t/\alpha) + i\zeta + \mathcal{O}(t^{-1})$, where $\Delta\varepsilon = \gamma^2/(2\pi v_F)^2 v_F t/\alpha$ and $\zeta = \gamma^2/(8\pi v_F^2)$ are real constants. The important property of \tilde{L}_2 is that it does not contain any real term proportional to t , i.e. it does not contribute to the exponential decay, but only to the OC. Summing up, we have

$$\tilde{\mathcal{L}}(t) = e^{-iE_{FS}t - \frac{\gamma}{2}\bar{n}t + \tilde{L}_2(t) + \mathcal{O}(\gamma^3)} \sim e^{i\zeta - i(E_{FS} + \Delta\varepsilon)t - \frac{\gamma}{2}\bar{n}t + \beta_b \ln(v_F t/\alpha) + \mathcal{O}(\gamma^3, t^{-1})}, \quad (42)$$

which decays exponentially, as advertised earlier, with a decay constant $\tilde{\Gamma} = \gamma\bar{n}/2 + \mathcal{O}(\gamma^3)$. A calculation along the same lines as the previous shows that

$$\langle \tilde{\psi}(t)|\tilde{\psi}(t)\rangle^{1/2} = e^{-\frac{\gamma}{2}\bar{n}t + 2\text{Re}\tilde{L}_2(t) + \mathcal{O}(\gamma^3)} \sim e^{-\frac{\gamma}{2}\bar{n}t + 2\beta_b \ln(v_F t/\alpha) + \mathcal{O}(\gamma^3, t^{-1})}. \quad (43)$$

These perturbative calculations show a number of relevant points. First, we see that both numerator and denominator decay exponentially, but with the *same* exponent $-\gamma\bar{n}/2$, so that this leading behavior disappears from the result:

$$\mathcal{L}(t) = \frac{\tilde{\mathcal{L}}(t)}{\langle \tilde{\psi}(t)|\tilde{\psi}(t)\rangle^{1/2}} \sim e^{i\zeta - i(E_{FS} + \Delta\varepsilon)t - \beta_b \ln(v_F t/\alpha) + \mathcal{O}(\gamma^3, t^{-1})}, \quad (44)$$

which agrees with the predictions from bosonization. Second, both $\tilde{\mathcal{L}}(t)$ and the state norm display an OC-like contribution in the form of a power-law growth, instead of a decay. An analogous behavior was observed in [12] in a dissipative context. In our case, the usual algebraic decay is recovered once the state is normalized. The third aspect is that we find no sign of the decay rate Γ that we measured in the numerics, which implies that it has to appear at a perturbative order larger than the second. Unfortunately, the cumulants of third and higher orders do not lend themselves easily to analytic calculations, so we have not been able to extract an expression for Γ . Moreover, we have argued that Γ may not be an analytic function in γ , so trying to compute it from any finite number of cumulants might be doomed to failure⁸. Nevertheless, in the main text we have found that Γ is far smaller than $\gamma\bar{n}/2$, and thus it would represent only a small correction to the leading decay of the return amplitude if we did not normalize the state. We conclude that the setup of post-selected measurements, and the nonlinear state evolution that it entails, is crucial to reveal the beyond-TLL behavior.

⁸ Cumulant expansions are also known for being possibly unstable beyond the lowest perturbative order.

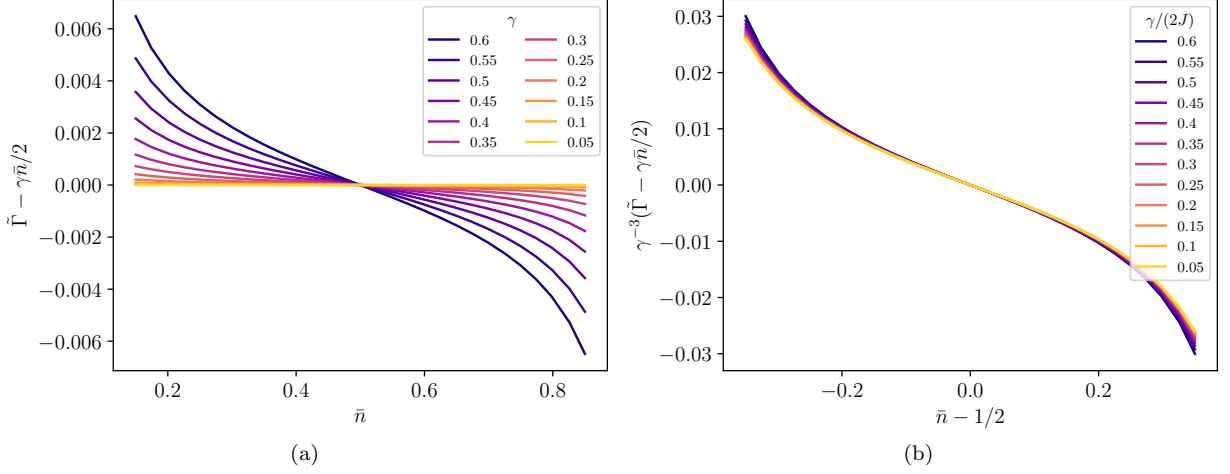


FIG. 10. Exponential decay rate of $\tilde{\mathcal{L}}(t)$, $\tilde{\Gamma} \equiv -\text{Im} \Delta E$, computed from the numerical diagonalization of the single-particle version of K for $L = 500$ sites, with $2J = 1$. (a) As a function of the density, showing the decreasing behavior once the average behavior $\gamma\bar{n}/2$ is subtracted. (b) Collapse of the data at different γ s, showing that $\tilde{\Gamma} - \gamma\bar{n}/2 = \mathcal{O}(\gamma^3)$.

Exact relations

There exist exact (i.e. non-perturbative in the impurity potential) calculations of the return amplitude for the Hermitian OC problem [26, 27], that prove its algebraic decay. In particular, the approach of [26] calculates $\langle FS | e^{-i(H+Vn_0)t} | FS \rangle$ from the spectral properties of the (Hermitian) OC Hamiltonian $H + Vn_0$, which are analogous to the non-Hermitian one in the $\gamma < 4J$ regime. Since these calculations express everything in terms of the scattering phase δ_p , which enters only through analytic functions, we can employ their results directly for our case with a complex δ_p . As stated in the main text, the main result of Ref. [26] that we need is that the “unrenormalized” return amplitude $\tilde{\mathcal{L}}(t) \equiv \langle FS | \tilde{\psi}(t) \rangle = \langle FS | e^{-iKt} | FS \rangle$ has the following asymptotic form at large times:

$$\ln \tilde{\mathcal{L}}(t) \sim -i\Delta E t - \beta \ln(\alpha t), \quad (45)$$

where α is a UV cutoff and the two constants are completely determined by the scattering phase:

$$\Delta E = \sum_{p \in FS} (\lambda_p - \varepsilon_p) = -\frac{2\pi}{L} \sum_{p \in FS} v_p \frac{\delta_p}{\pi} = -\int_{-2J}^{\varepsilon_F} d\varepsilon \frac{\delta(\varepsilon)}{\pi}, \quad (46a)$$

$$\beta = \frac{\delta_{k_F}^2}{\pi^2} = \frac{\delta(\varepsilon_F^2)}{\pi^2}, \quad (46b)$$

where $\delta(\varepsilon)$ is the scattering phase expressed in terms of the energy $\varepsilon = \varepsilon_p$ in the continuum limit. In these calculations it is convenient to symmetrize the momentum states as in Eq. (14). In this way only the symmetric modes interact with the impurity and we can work in the half-Brillouin zone $p \in \{\frac{2\pi n}{L} | n = 0, 1, \dots, \frac{L}{2}\}$, where the dispersion relation $\varepsilon = \varepsilon_p$ is invertible. In the Hermitian scenario, the two constants ΔE and β have very different roles—the former contributing to an overall phase while the latter gives the algebraic decay of the modulus of $\tilde{\mathcal{L}}(t)$. In the present, non-Hermitian case, δ_p is complex, so that both the modulus and the phase of $\tilde{\mathcal{L}}(t)$ receive contributions from each of the terms. We have already commented on the properties of β and ΔE in the main text. Here we report a more in-depth discussion of the properties of the exponential decay rate of $\tilde{\mathcal{L}}(t)$, $\tilde{\Gamma} \equiv -\text{Im} \Delta E$. We show $\tilde{\Gamma}$ in Fig. 10, computed from the numerical diagonalization of K . The left panel shows that if we subtract the leading term $\gamma\bar{n}/2$, we obtain a correction monotonically decreasing with the density. Indeed, since $\tilde{\Gamma}_b = \gamma\bar{n}/2$ is the prediction of bosonization, this correction is already a beyond-TLL effect. Although the qualitative behavior is the same as Γ (i.e. the decay rate of the true return amplitude), the quantitative relation is different, since $\tilde{\Gamma} - \gamma\bar{n}/2$ can be fitted to an odd polynomial in $(\bar{n} - 1/2)$. The left panel shows the collapse of the curves at different γ s by rescaling them by γ^3 , which suggests an overall form

$$\tilde{\Gamma} \approx \frac{\gamma}{2}\bar{n} + \gamma^3 \left[a_1 \left(\bar{n} - \frac{1}{2} \right) + a_3 \left(\bar{n} - \frac{1}{2} \right)^3 \right], \quad (47)$$

for certain coefficients $a_{1,3}$. This discussion is meant to illustrate concretely how the density can enter nontrivially in the return amplitude. It also shows that the behavior that we observed in Γ for the full return amplitude ultimately depends on the interplay between $\tilde{\mathcal{L}}(t)$ and the norm of the state $\langle \tilde{\psi} | \tilde{\psi} \rangle^{1/2}$.

Unfortunately, the results of Ref. [26] can not be used to compute the $\langle \tilde{\psi} | \tilde{\psi} \rangle$, but we can still make some useful remarks on its behavior. It is easy to prove that

$$\langle \tilde{\psi} | \tilde{\psi} \rangle^{1/2} = e^{-\frac{\gamma}{2} \int_0^t dt' \langle n_0 \rangle(t')} , \quad (48)$$

by direct differentiation. If, as observed in Fig. 3, $\langle n_0 \rangle(t)$ tends to a constant⁹, n_∞ , then the full decay rate is $\Gamma = \tilde{\Gamma} - \gamma n_\infty/2$, and the observed exponential decrease of Γ with the density is equivalent to say that $\gamma n_\infty/2$ tends to $\tilde{\Gamma}$ for increasing \bar{n} . This is indeed confirmed by the numerical data.

Comparison with localized dephasing

We complement the previous discussion on the role of post-selection by comparing the result for the non-Hermitian OC with its closest dissipative analogue—the case of localized dephasing, defined by the master equation

$$\frac{d}{dt} \rho(t) = -i[H, \rho(t)] + \gamma(n_0 \rho(t) n_0 - \frac{1}{2}\{n_0, \rho(t)\}) . \quad (49)$$

This model has been already considered in [11, 12], and it can be obtained from the dynamics induced by the measurement operators (3) if the state is averaged on the measurement outcomes, thus eliminating any post-selection. As noted at the beginning of this Supplementary Material, the master equation (49) shares the same non-Hermitian Hamiltonian $K = H - i\gamma n_0/2$ part of the dissipative dynamics as the nonlinear Schrödinger equation (1). We can simulate the dynamics of Eq. (49) efficiently with the same algorithm used in this work, because it is equivalent [11] to the stochastic dynamics induced by a noisy (real) impurity

$$H_\xi(t) = H + \gamma^{1/2} \xi(t) n_0 , \quad (50)$$

where $\xi(t)$ is a Gaussian white noise defined by the correlator $\overline{\xi(t)\xi(t')} = \delta(t-t')$ ($\overline{\cdot}$ is the noise average). Then, the state $\rho(t)$ evolving with Eq. (49) is obtained by averaging the state $\rho_\xi(t) = |\psi_\xi(t)\rangle\langle\psi_\xi(t)|$ evolved with $H_\xi(t)$ over the realizations of the noise. Since $H_\xi(t)$ is quadratic (unlike the time evolution induced by the master equation), we can apply the stochastic version of the algorithm in Ref. [20].

We can anticipate that we will not find any monotonic behavior in the density, since Eq. (49) is ph-symmetric—it is easy to verify that $\mathcal{C}\rho(t)\mathcal{C}^\dagger$ satisfies the same equation as $\rho(t)$. Thus, we expect that all the quantities will be invariant under the exchange $\bar{n} \rightarrow 1 - \bar{n}$. Indeed, this is what we observe from the numerics, as shown in Fig. 11. Figure 11a shows the Loschmidt echo, which is the average of the squared modulus of the return amplitude, $|\langle FS | \psi_\xi(t) \rangle|^2 = \langle FS | \rho(t) | FS \rangle$, while Fig. 11b shows the absorbed energy $E(t) = \text{Tr}[\rho(t)H]$. In both Figures we observe a perfect ph symmetry, such that the data for conjugate densities (\bar{n} , $1 - \bar{n}$) coincides within the scale of the Figures (the differences are of the same order of magnitude as the residual randomness in the averaged data). On a qualitative level, we notice that the Loschmidt echo decays much faster than in the post-selected setting, owing to a decay rate which is linear in γ to the leading order [12] $\Gamma_{\text{deph}} = \frac{1}{2}\gamma\bar{n}(1 - \bar{n}) + \mathcal{O}(\gamma^3)$ (which has a ph-symmetric dependence on the density, of course). This fast exponential decay overshadows the $\mathcal{O}(\gamma^2)$ algebraic behavior predicted in [12]. The behavior of the energy (Fig. 11b) is qualitatively similar to the post-selected setup, except that the growth rate is two order of magnitude larger—in accord with the fast decay of the Loschmidt echo. In Fig. 11c we show the average occupation in momentum space, for different densities. The behavior is quite different from that of the post-selected scenario, with a Fermi sea that is significantly depleted from the outside in. The possibility of a relation between the two momenta which seem more resistant to dissipation and the special modes q^* requires further investigations.

[1] H. M. Wiseman and G. J. Milburn, *Quantum Measurement and Control* (Cambridge University Press, Cambridge, 2009).

⁹ By comparing Eq. (48) with $\ln |\tilde{\mathcal{L}}(t)| \sim -\tilde{\Gamma}t + \beta \ln t + \mathcal{O}(1)$ and $\ln |\mathcal{L}(t)| \sim -\Gamma t - \beta \ln t + \mathcal{O}(1)$, we obtain $\langle n_0 \rangle(t) \sim n_\infty + 4\beta/(\gamma t) + \mathcal{O}(t^{-2})$.

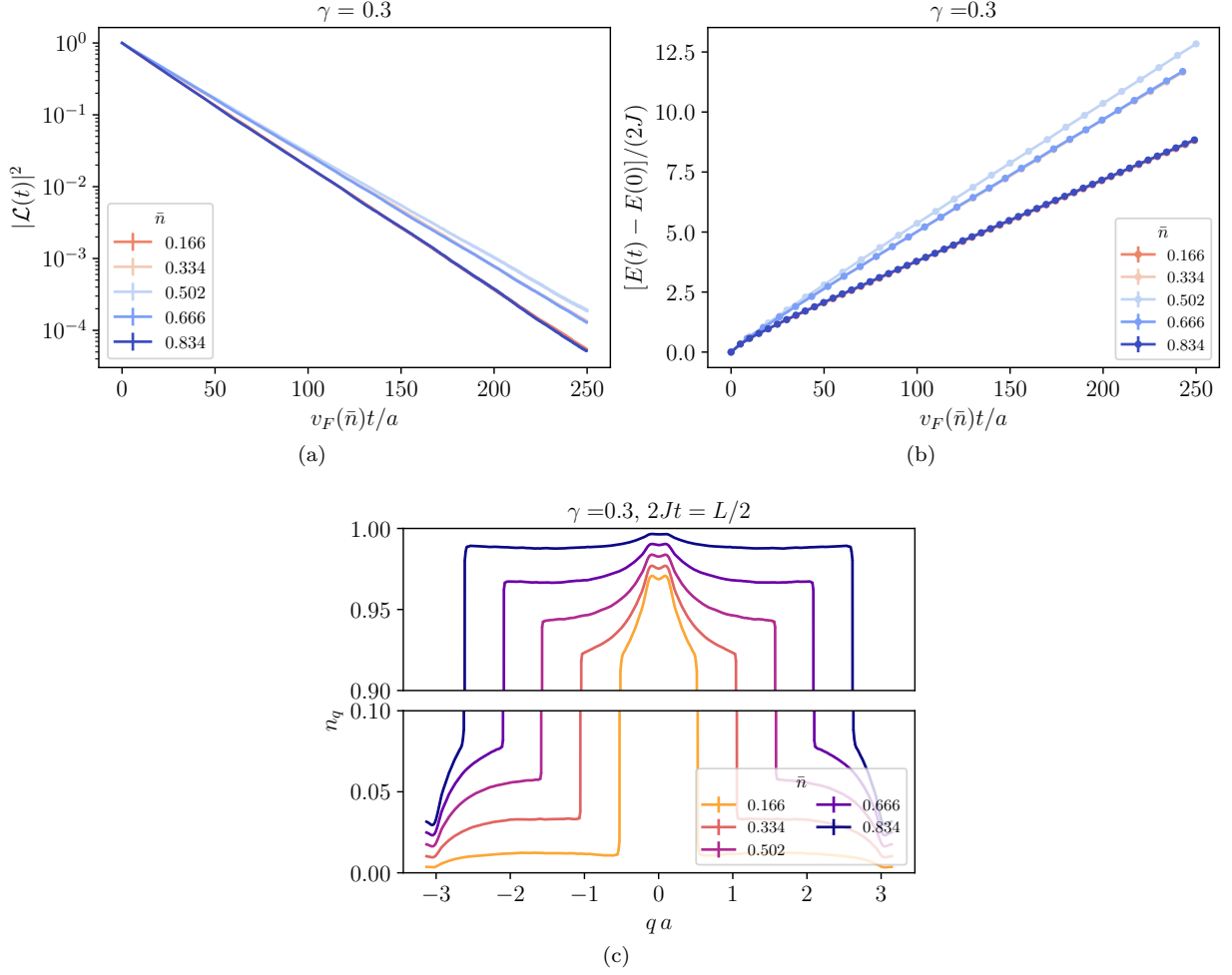


FIG. 11. Properties of a system with $L = 500$ sites subjected to measurements (3) without post-selections, namely local dephasing [Eq. (49)]. (a) Average square of the return amplitude, i.e. the Loschmidt echo $\langle FS|\rho(t)|FS\rangle$. (b) Average energy absorption. (c) Occupation of the momentum modes for varying density. The plots have been obtained by averaging 1024 trajectories generated by $H_\xi(t)$. The error bars are calculated as the standard deviation of the empirical mean, which is comparable with the thickness of the lines.

- [2] S. J. Garratt, Z. Weinstein, and E. Altman, Measurements conspire nonlocally to restructure critical quantum states (2022), [arXiv:2207.09476 \[cond-mat.stat-mech\]](#).
- [3] X. Turkeshi and M. Schiró, Entanglement and correlation spreading in non-Hermitian spin chains, *Phys. Rev. B* **107**, L020403 (2023).
- [4] Y. Le Gal, X. Turkeshi, and M. Schiró, Volume-to-area law entanglement transition in a non-Hermitian free fermionic chain, *SciPost Phys.* **14**, 138 (2023).
- [5] X. Turkeshi, A. Biella, R. Fazio, M. Dalmonte, and M. Schiró, Measurement-induced entanglement transitions in the quantum Ising chain: From infinite to zero clicks, *Phys. Rev. B* **103**, 224210 (2021).
- [6] H. F. Fröml, *Localized dissipation in fermionic quantum wires*, Ph.D. thesis, Universität zu Köln (2020).
- [7] H. Fröml, A. Chiocchetta, C. Kollath, and S. Diehl, Fluctuation-induced quantum zeno effect, *Phys. Rev. Lett.* **122**, 040402 (2019).
- [8] H. Fröml, C. Muckel, C. Kollath, A. Chiocchetta, and S. Diehl, Ultracold quantum wires with localized losses: Many-body quantum zeno effect, *Phys. Rev. B* **101**, 144301 (2020).
- [9] T. Müller, M. Gievers, H. Fröml, S. Diehl, and A. Chiocchetta, Shape effects of localized losses in quantum wires: Dissipative resonances and nonequilibrium universality, *Phys. Rev. B* **104**, 155431 (2021).
- [10] P. L. Krapivsky, K. Mallick, and D. Sels, Free fermions with a localized source, *J. Stat. Mech.*, 113108 (2019).
- [11] P. E. Dolgirev, J. Marino, D. Sels, and E. Demler, Non-gaussian correlations imprinted by local dephasing in fermionic wires, *Phys. Rev. B* **102**, 100301 (2020).
- [12] F. Tonielli, R. Fazio, S. Diehl, and J. Marino, Orthogonality catastrophe in dissipative quantum many-body systems, *Phys. Rev. Lett.* **122**, 040604 (2019).

- [13] G. D. Mahan, *Many-Particle Physics*, 2nd ed. (Plenum press, New York, 1993).
- [14] T. Giamarchi, *Quantum Physics in One Dimension*, 1st ed. (Clarendon Press, Oxford, 2003).
- [15] A. O. Gogolin, A. A. Nersisyan, and A. M. Tsvelik, *Bosonization and Strongly Correlated Systems* (Cambridge University Press, Cambridge, 1998).
- [16] M. Knap, A. Shashi, Y. Nishida, A. Imambekov, D. A. Abanin, and E. Demler, Time-dependent impurity in ultracold fermions: Orthogonality catastrophe and beyond, *Phys. Rev. X* **2**, 041020 (2012).
- [17] B. Yan, S. A. Moses, B. Gadway, J. P. Covey, K. R. A. Hazzard, A. M. Rey, D. S. Jin, and J. Ye, Observation of dipolar spin-exchange interactions with lattice-confined polar molecules, *Nature* **501**, 521 (2013).
- [18] B. Zhu, B. Gadway, M. Foss-Feig, J. Schachenmayer, M. L. Wall, K. R. A. Hazzard, B. Yan, S. A. Moses, J. P. Covey, D. S. Jin, J. Ye, M. Holland, and A. M. Rey, Suppressing the loss of ultracold molecules via the continuous quantum zeno effect, *Phys. Rev. Lett.* **112**, 070404 (2014).
- [19] K. Sponselee, L. Freystatzky, B. Abeln, M. Diem, B. Hundt, A. Kochanke, T. Ponath, B. Santra, L. Mathey, K. Sengstock, and C. Becker, Dynamics of ultracold quantum gases in the dissipative fermi-hubbard model, *Quantum Sci. Technol.* **4**, 014002 (2018).
- [20] X. Cao, A. Tilloy, and A. D. Luca, Entanglement in a fermion chain under continuous monitoring, *SciPost Phys.* **7**, 024 (2019).
- [21] C. L. Kane, K. A. Matveev, and L. I. Glazman, Fermi-edge singularities and backscattering in a weakly interacting one-dimensional electron gas, *Phys. Rev. B* **49**, 2253 (1994).
- [22] A. Imambekov, T. L. Schmidt, and L. I. Glazman, One-dimensional quantum liquids: Beyond the Luttinger liquid paradigm, *Rev. Mod. Phys.* **84**, 1253 (2012).
- [23] S. Blanes, F. Casas, J. Oteo, and J. Ros, The magnus expansion and some of its applications, *Physics Reports* **470**, 151 (2009).
- [24] Y. Ashida, Z. Gong, and M. Ueda, Non-Hermitian physics, *Advances in Physics* **69**, 249 (2020).
- [25] P. C. Burke, J. Wiersig, and M. Haque, Non-Hermitian scattering on a tight-binding lattice, *Phys. Rev. A* **102**, 012212 (2020).
- [26] M. Combescot and P. Nozières, Infrared catastrophe and excitons in the X-ray spectra of metals, *J. Phys. (France)* **32**, 913 (1971).
- [27] P. Nozières and C. T. De Dominicis, Singularities in the X-ray absorption and emission of metals. iii. one-body theory exact solution, *Phys. Rev.* **178**, 1097 (1969).